Kettlectric and myGen: Portable, Thermoelectric-Based Power Generation Systems for Off-Grid Home Use and the Village Entrepreneur

Michael Charles Kozlowski

Bachelor of Science in Mechanical Engineering
Massachusetts Institute of Technology, 2008

Submitted to the Department of Mechanical Engineering
in partial fulfillment of the requirements for the degree of

MASTER OF SCIENCE IN MECHANICAL ENGINEERING

at the

MASSACHUSETTS INSTITUTE OF TECHNOLOGY

MAY 2010
[June 2010]

Author . . . . . .
Department of Mechanical Engineering
May 9, 2010

Certified by . . . . . .
Amy B. Smith
Senior Lecturer of Mechanical Engineering
Thesis Supervisor

Certified by . . . . . .
Gang Chen
Carl Richard Soderberg Professor of Power Engineering
Thesis Supervisor

Accepted by . . . . . .
David E. Hardt
Chairman, Committee on Graduate Students

Kettlectric and myGen:
Portable, Thermoelectric-Based Power Generation Systems for Off-Grid Home Use and the Village Entrepreneur

by
Michael Charles Kozlowski

Submitted to the Department of Mechanical Engineering
on May 7, 2010, in partial fulfillment of the
requirements for the degree of
MASTER OF SCIENCE IN MECHANICAL ENGINEERING

Abstract

There are 1.6 billion people across the globe who still live without access to electricity. For this group, the modern electrical framework providing fundamental services for health, food and water processing and storage, sanitation, and communication is often out of reach. As a result, many suffer negative health, social, and economic consequences.

In response, many have spurred electrification initiatives using conventional and renewable energy technologies as well as market-based approaches. However, few have considered thermoelectric technology in this context despite its capacity for long-lasting, solid-state electricity production directly from heat energy. The current work investigates such application for small-scale, off-grid power generation.

Several systems were prototyped that are capable of generating electricity as a by-product of cooking. *Kettlectric* was the first developed and is based on a kettle design. It can produce 1.8 watts of peak power (Wp) and is compatible with off-the-shelf mobile rechargers and LED task lights by using a battery intermediate.

After field study in Tanzanian, two additional *myGen* systems were constructed using separate manufacturing techniques. As pot retro-fits, they are adaptable to almost every observed cooking environment. Unlike Kettlectric, which boils water for a specific end-use, the myGen systems are single-function units that do not interfere with cooking habits. Each is capable of about 2 Wp of output and could potentially be scaled-up to provide income generation.

The Kettlectric and myGen prototypes demonstrate functionality for small-scale, off-grid power generation systems, but successful dissemination is contingent upon significant decreases in thermoelectric module cost. However, reduced prices are expected in the coming years as demand for these devices increases.

Thesis Supervisors: Amy Smith and Gang Chen

Kettlectric and myGen:
Portable, Thermoelectric-Based Power Generation Systems for Off-Grid Home Use and the Village Entrepreneur

by

Michael Charles Kozlowski

Acknowledgements

I would like to take this opportunity to thank those who have made this thesis possible. Most tangibly, Mike Tarkanian, Dennis Nagle, Mark Bellanger, Pat McAtamney, Dave Dow, and Aurthur Anthony of Mystic Valley Foundry, who each helped tremendously in the fabrication of prototypes. I am also grateful for the assistance of Angela Mickunas and Paula Cogliano, especially in facilitating travels to Saudi Arabia and Tanzania. Thanks is also extended to my advisers, Amy Smith and Gang Chen, for their feedback, encouragement, and support; working with these influential leaders has been a valuable and enjoyable experience. In addition, my lab mates from D-Lab and the Nanoengineering Group were present throughout, for support and engagement both academically and socially. Finally, funding through the MIT-KFUPM Clean Water and Clean Energy research collaboration is very much appreciated.

Mike Kozlowski
Cambridge, MA
May 9, 2010

Contents

1 Introduction **5**
- 1.1 Technical Feasibility . . . 7
- 1.2 Customer Requirements . . . 10
- 1.3 Market Analysis and Selection . . . 11

2 Product Design: Modeling, Laboratory Testing, and Experimental Results **15**
- 2.1 Development and Description of a Simulation Environment . . . 16
  - 2.1.1 Flame-Source Modeling . . . 16
  - 2.1.2 Heating Characterization and Stove Analog Selection . . . 19
- 2.2 Power Generation System . . . 23
  - 2.2.1 The Steam Pipe Approach . . . 23
  - 2.2.2 Kettle External Enclosures . . . 24
  - 2.2.3 Internal Module Clamping: The Water Barrier Method and Kettlectric . . . 32
- 2.3 Selecting a Thermoelectric Module . . . 40
- 2.4 Charge Control and Storage System . . . 43
  - 2.4.1 Storage Devices . . . 43
  - 2.4.2 Charge Control Circuitry . . . 44
  - 2.4.3 Battery Safety . . . 46
- 2.5 End-Use Applications . . . 47
  - 2.5.1 Lighting . . . 47
  - 2.5.2 Mobile Phone Charging . . . 49

3 Field Testing and Product Re-Design **51**
- 3.1 An Improved Customer Understanding . . . 52
- 3.2 Abandoning Kettlectric: An Appropriate System . . . 54
  - 3.2.1 myGen: A Side-Mount Design . . . 55
  - 3.2.2 The Box Extrusion myGen . . . 59
  - 3.2.3 myGen Manufacturing . . . 60

4 Final Conclusions and Future Work **62**

Chapter 1

Introduction

The global supply of energy is not distributed equitably. Developing countries account for 80% of the world's population yet consume only 30% of the global commercial energy supply [1]. Of the worldwide electrical capacity of 3.4 TW in 2000, developing countries consumed only 1.5 TW, or 45% [1,2]. In rural areas, consumption is generally even lower, with only 2-5% of the population with access in much of sub-Saharan Africa, increasing to 20-30% for countries like Brazil, Bangladesh, India, Morocco, and South Africa [1]. Consequently, over 20% of the global population, or 1.6 billion people, live without access to the grid [3].

Nevertheless, some are able to find electricity, in most cases by traveling to grid access points or by utilizing diesel generators or solar installations. In Tanzania, for example, 80% of the population lives within 5 kilometers of a transmission line [4]. But in other locations, generators typically provide access and are generally used to power small shops and public buildings (e.g. local clinics). These are also used by local entrepreneurs who generate income by selling electricity [5]. Solar installations can be leveraged similarly, but are typically installed for personal use. Smaller units from 10-100 Wp (peak watts) can operate several lights, a black-and-white television, radio, and small fan. As of 2000, worldwide installation estimates reached 500,000 [6] with an almost doubling (to about 900,000) by 2002 [1]. Finally, by combining power sources such as diesel generators and hydro-turbines, mini-grids can be assembled to serve tens to hundreds of households per location in remote, off-grid villages. As of 2002, there were 60,000 in operation in China alone [1].

In addition to existing solutions for off-grid power generation, there are many emerging approaches

at both the large and small scales. One proposal is to expand the penetration of mini-grids by adapting them for use with other energy sources such as solar, wind, and biomass [1, 6]. Biofuel sources are particularly attractive since they can be grown locally, displacing costly imports and creating local value chains; fuel farms might also be models for sustainable growing practices [7]. Biofuels can also be coupled with fuel cells for direct electricity production [8], which is one of the strategies of Bloom Energy, a US-based startup. They have created a power generation unit called the Bloom Box that can operate using a multitude of fuel inputs [9, 10]. Their fuel cells are manufactured using a common "sand-like" powder which may decrease cost, making these systems more affordable [9, 10]. With a different approach, EGG Energy is promoting a market-based battery swapping scheme where users rent rechargeable batteries and exchange them when they have been depleted [11].

At the smaller scale, several start-ups are seeking to exploit solar, microbial fuel cell, and wind energy sources. The Mighty Light, for example, provides 30 years of quality LED lighting with a $45 solar lantern. This product was launched from the US-India lab Cosmos Ignite Innovation and has been used in Afghanistan, Guatemala, India, Pakistan, and Rwanda [8]. D.Light Design is another solar-based company offering lighting and mobile charging solutions. They have reached "one million lives impacted through solar lighting" as of March 2010 [12]. On another front, Lebone Solutions is offering an extremely simple microbial fuel-cell system made of common items such as manure, soil, and wire [8]. Finally, Humdinger Wind Energy is taking a new approach on wind harnessing. Their devices use a resonating band which oscillates a magnet near a coil to generate electricity [13]. Their small unit, with a belt on the order of 10 cm in length, can produce 1 mW - 1 W in 6-20 mph winds, while the medium-sized versions (1 m band length) can output 1-100 W under similar conditions [13].

Finally, thermoelectric technology has been utilized for off-grid applications, but sparingly, likely due to a high cost/output ratio (see Table 1.1). Power generation modules have been integrated with cooking stoves for improved combustion efficiency (by powering an oxygen-feeding fan) and power generation using both air [14, 15, 16, 17] and liquid [18] cooling. Others [19, 20] have demonstrated their use with cooking pots for simultaneous power generation.

Table 1.1: Cost per output for several of the systems mentioned. The dollar value was taken as the capital cost of the system only, and does not include consumables such as fuel or batteries.

	Capital Cost $	Power Output W	Cost/Output $/W	Source
Small-scale systems (< 50 W)				
Fluorescent Solar Lantern	30	5	6.0	[21]
Two-Battery Flashlight	5	0.75	6.7	[21]
Thermoelectric System[a]	40	3.5	11.4	[19]
LED Solar Lantern	25	1	25.0	[21]
Large-scale systems (> 50 W)				
Diesel Generator	1,300	4,000	0.3	[22]
Bloom Box	750,000	100,000	7.5	[23]
School Solar Installation[b]	4,500	400	11.3	[24]
Home Solar Installation[c]	1,000	50	20.0	[25]

[a] Capital price is a projected system cost assuming (i) the module accounts for 75% of material cost, (ii) the retail price is four times the manufacturing cost, and (iii) quantities are on the order of 10,000. Power output was measured in the laboratory under expected operating conditions.

[b] System cost from the director of the Indigenous Education Foundation of Tanzania. Output was estimated based on usage.

[c] Price and power output estimates from a field partner living in a Ngorongoro Massai village in Tanzania.

Although cost/output is high for thermoelectric systems, it is not prohibitively so and this platform offers a number of other benefits. Thus, the the aim of the current work is to use thermoelectric technology as the basis for a personal scale, off-grid power generation system. It will function by using heat energy from a cooking fire with an open water reservoir for cooling, allowing operation in almost any environmental conditions. Because the thermoelectric module is a solid-state device, the system is expected to be reliable for up to twenty years with little maintenance required and minimal performance degradation over time [26]. By developing the system at this time, implementation can quickly follow a decrease in cost, avoiding any significant distribution lag once the thermoelectric price-point is reached.

1.1 Technical Feasibility

At the core of the power generation system is the thermoelectric module, which functions using semiconductor materials. Unlike metals, which conduct electricity via electrons only, semiconduc-

tors carry charge with both electrons and "holes" (the absence of electrons). When doped with elements having additional valence electrons, the semiconductor becomes an n-type material, conducting through the flow of electrons. On the other hand, doping with elements having fewer valence electrons creates holes in the material, and flow is sustained with mobilized positive charge [27]. For both material types, carrier motion can be triggered with energy input, whether electrical or thermal. Thus, when n- and p-type segments are coupled appropriately, current can flow through both materials uniformly. Figure 1.1(a) shows such a configuration, where both material types are configured thermally in parallel and electrically in series. When heat is added at one junction, elec-

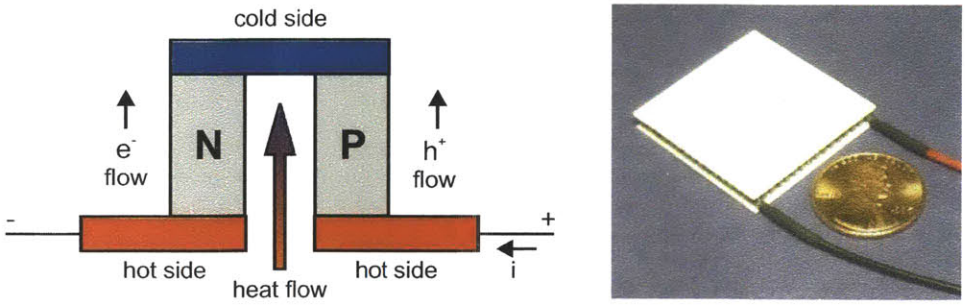

(a) (b)

Figure 1.1: Many semiconductor couples of (a) are assembled into arrays to form complete modules such as shown in (b) (image from eHow [28]).

trons in the n-type material and holes in the p-type are driven to the cold side. Thus the coupling of n- and p-type semiconductor materials in this manner creates a flow of current, converting heat energy directly to electricity [29,30,31]. To increase power output to a useable level, many couples are arranged in an array to form a complete module, as shown in Figure 1.1(b). When the module is connected in a circuit, its internal resistance should match that of the load in order to maximize power output and efficiency.

To determine whether such modules are capable of providing adequate output for the system, power requirements of end-use devices must first be quantified. Amongst LED task lights, mobile phones, and personal radios, the latter have the least power requirements, with laboratory measurements of 40 mW of power consumption when the volume is set to a moderate listening level. For a task light, LEDs typically draw about 20 mA at a minimum of 3 VDC [32,33]; thus, for a five and ten LED light, power requirements reach 300 and 600 mW. Finally, mobile phones draw about 275

and 2.5 mA at 3.7 VDC for talk time and standby-mode conditions, respectively, corresponding to about 1000 and 9 mW of power consumption [34]. These estimates serve as reference points for evaluating thermoeletric output.

Manufacturer data suggest module output can range from about 1-6.5 W depending on size and operating conditions [19,35,36,37]. To pick one, a 40 x 40 mm module (p/n TEP1-1264-1.5) from the Chinese manufacturer Thermonamic [19] is quoted for about 6 W of output given a temperature differential of 200°C and a heat flow of 140 W. For the proposed generation system, the maximum low-temperature side will reach 100°C during boiling, thus requiring 300°C on the high temperature side to achieve the 200°C differential[1]. This is possible given the module's ability for continuous operation at up to 320°C [19]. Note that water will be used for cooling instead of air because the process is passive (air cooling would require the use of a fan) and more effective.

Meeting the heat flow requirement is also achievable. Given a lower-heating value (LHV) of 12 MJ/kg for air-dry wood [38] and a burn of 1 kg of fuel over 30 minutes and 960 square centimeters[2], the fire heat flux is estimated to be 7 $\frac{W}{cm^2}$. In order to achieve the flow of 140 W through the module, only 20 cm^2 is required for heat collection.

Assuming a module output of 3 W, half of the manufacturer's claim, the end-use applications look promising. Given adequate intermediate storage, thirty minutes of generation time at 3 W of output would provide enough energy for over 35 hours of radio use, 2.5 hours of lighting with a ten LED system, or five hours of lighting with a five LED lamp; this amount of energy could also provide 1.5 hours of mobile talk-time or over 150 hours of power in standby mode[3].

In order to store this much energy, a battery or alternative technology must be used, with capacity for 5400 J (3W for 30 minutes). Generally, rechargeable battery packs consist of three cells with each providing 1.25 V, thus totaling 3.75 V. In this case, the capacity for each would have to be

[1]This requirement assumes that module output will be the same regardless of where the temperature range lies. This is likely not the case, but serves as a reasonable estimate to assess feasibility.

[2]This is about 1.5 times the area of a standard Tanzanian cooking pot. The calculation assumes that the fire will extend slightly over the projected area of the pot.

[3]Note that efficiency in the electrical circuits was not taken into account for ease of calculation. The final values for end-use time would be lower than those estimated here.

Table 1.2: Product specifications based on the predicted requirements of the intended customer.

Customer Need	Product Attribute	Product Specifications		
		metric	*value*	*units*
Performs as cooking analog	cook time	added time	< 5	minutes
	capacity	added volume	< 10	%
	washability	post function	yes	binary
	durability	lifetime reduction	< 2	years
Locally available	affordability	cost	< 30	$
Should not cause burns	cool interactions sites	temperature	< 50	°C
Chemically stable	battery pack	catastrophic failures	0	count
Generates power	TE module	power output	> 1.5	W
Stores useable energy	battery pack	energy	> 200	mAh

at least 400 mAh, an easy requirement considering typical AAA rechargeables can store over 700 mAh [33]. With voltage-boosting circuits, fewer cells might be used to achieve the necessary storage capacity.

Based on these preliminary findings, it seems that the proposed solutions of using a thermoelectric power generation module to charge re-useable batteries to then power end-use devices such as mobile phones, task lights, and radios is technically feasible. Users could experience the benefits of these devices with only a short charge of the system each day.

1.2 Customer Requirements

In designing an appropriate product, it is crucial that customer needs are fully understood. Collection of this information is best done through direct user interaction and observation. However, given the geographic location of intended users, a set of best-judgement requirements was compiled from various interactions with colleagues of D-Lab at MIT[4], a group well-versed in developing appropriate technologies. The resulting product specifications are shown in Table 1.2. In general, the needs and product attributes presented are self-explanatory. These describe a cooking vessel to be used as a standard one, but that can also generate and store electrical energy in a safe manner.

[4]Unfortunately, these personal interactions were too numerous and brief to cite them all.

Note that 1.5 W was selected as the power output requirement in order to achieve at least 200 mAh of storage for 30 minutes of generation time. This would be enough energy to light five ultra-bright LEDs for about two hours (again, assuming perfect electronic efficiencies).

In addition to customer needs and product specifications, there are other design requirements that follow from the items shown in the table. For example, minimizing cook time implies reduced fuel consumption. Also, the system must be adaptable for various heating conditions (e.g. gas stove, biomass fire), which might be categorized under the "Performs as analog" heading.

To ensure an extended product lifetime, the design must prevent again two critical failure modes. The first will be termed "dry boil" in which the cooling water completely boils-off, causing overheating of the system and degradation of the thermoelectric module. The second overheating condition would occur if the user places the system directly on hot coals, since heat will be transferred by direct conduction instead of through convection.

However, information collected regarding these failure modes suggests that they are unlikely to occur. Fuel is precious and homes are small, motivating the user to remain near the fire, guarding against dry boil, so to speak [39]. Similarly, failure by hot-coal conduction is unlikely given the ubiquitous nature of cooking by convection [39, 40]. Nevertheless, a safety feature should be incorporated into the system to prevent these worst-case scenarios.

1.3 Market Analysis and Selection

The proposed system is potentially useful across the globe. Currently, there are 1.6 billion people worldwide that are off-grid [21]: nearly 75% of sub-Saharan Africa and 50% of South Asia, representing a total of 1.25 billion people for these regions alone [41]. Further, many who are counted as having access do not utilize it. In India, for example, "official" reports indicate 85% electrification of villages, but fewer than 60% of rural households actually consume electricity since it is not directly available to each family [42]. Coupled with the lack of electricity is the tradition of

cooking over open fires, which is particularly relevant for the current product. In fact, more than three billion people worldwide use biomass fuels for cooking and heating [21].

Surprisingly, many of those living without electricity own electronic devices, most notably, the cell phone. In fact, nearly 500 million people own mobiles yet are forced to find alternative pay-per-use charging methods [43]. A personal charger to replace these services has been valued at $2.3 billion since it would increase talk time and thus average revenue per user [43]. Beyond mobiles, the system offers the potential for powering other life-improving devices such as clean lights and radios.

To deliver this product in an economically sustainable manner, a market-based dissemination approach is preferred. By identifying a customer willingness to pay beyond the cost to deliver the product, sales will occur without subsidy [44]. However, finding such a price will prove difficult given the relationship between income and electricity access. Figure 1.2 shows that those with the least access (highest demand) are the poorest (least ability to pay).

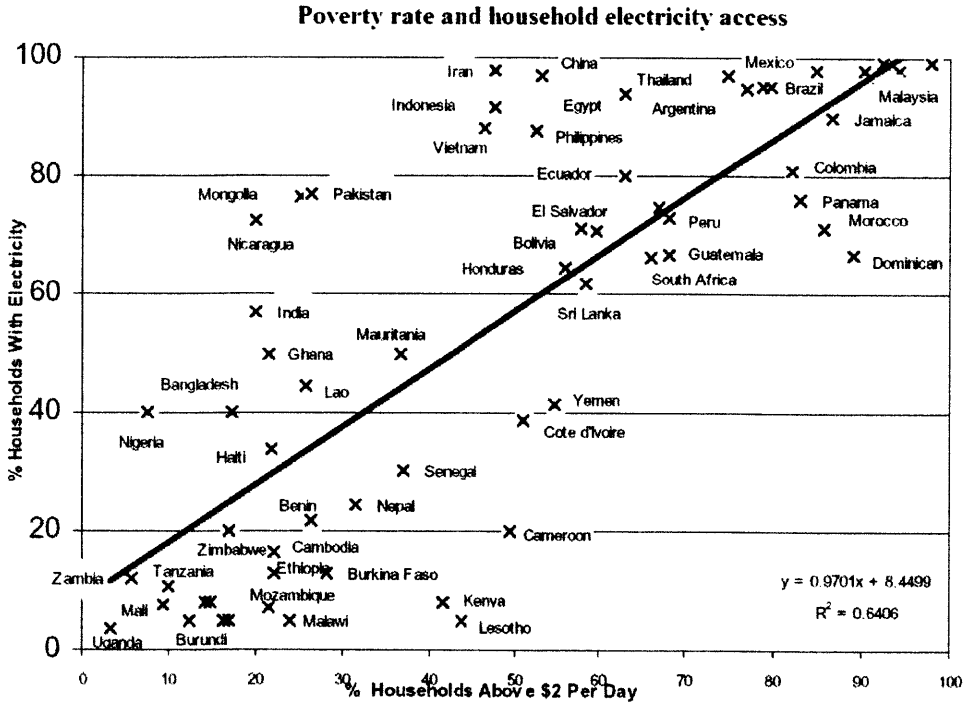

Figure 1.2: System cost must be as low as possible since those with the highest demand have the least ability to pay. *Figure from The World Bank [21].*

Table 1.3: A matrix of potential target countries with indication for purchasing power, off-grid inhabitants, and mobile subscribers. *Reproduced from Zira [45].*

Country	Climate	Rural Population %	Per Capita GDP PPP	Mobile Subscribers Million
Bolivia	varied	unknown	4345	4.4
Mexico	hot, temperate	25	14500	83
Tanzania	hot, dry	60	1353	14
Cambodia	hot, wet	65	2082	4
South Africa	temperate	50	10100	40
Tajikistan	cold	unknown	2000	3.5
Chile	varied	15	14500	18
Ghana	hot	unknown	1571	16
Brazil	humid, hot	15	10100	100
Peru	varied	30	7600	23
India	varied	71	2600	100

Nevertheless, it is helpful to identify target geographic locations for future dissemination. In basic terms, the ideal market would have many rural citizens with a relatively high average income. A location with poor climate might prove to be a non-competitive opportunity given the system's ability to operate in any weather conditions. As opposed to solar, for example, it will function at night or during rain provided a cooking fire can be sustained. Table 1.3 is a non-exhaustive list providing countries of interest, including climate, percentage of rural population, per capita GDP[5], and number of mobile subscribers. The data identify South Africa and Peru as places of interest. Both locations have a fairly high percentage of the population living in rural areas with a relatively higher per capita GDP. Although the South African climate is more temperate, it has a large number of mobile subscribers, suggesting a well-establish industry and network coverage. Peru may offer more fitting environmental conditions, but its mobile penetration is lower.

Although climate is not the main driver for market selection, it is interesting to further consider it. Because the system can function with only heat and water, it would be well-suited for cloudy locations, where solar systems are not effective. Figure 1.3 shows average worldwide cloud cover for February and June of 2009. Each figure was generated by "averaging" daily cloud-cover images

[5]Per capita GDP is a sub-optimal method for assessing income levels of the poor since wealth is not distributed equally in free societies. However, this measure was used as a rough indicator due to its widespread availability.

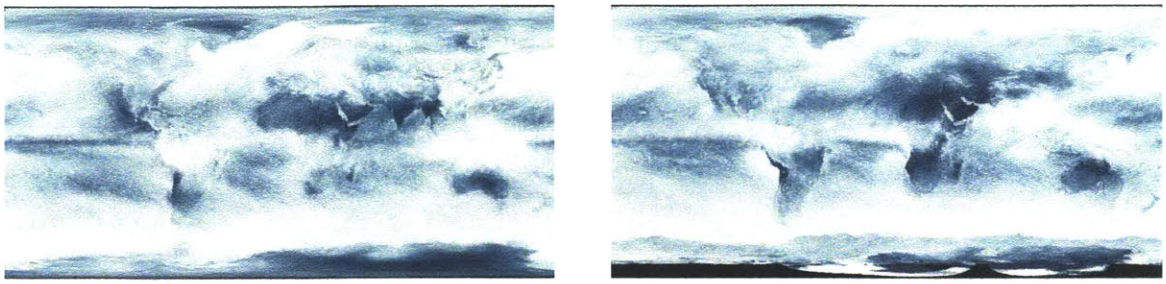

(a) (b)

Figure 1.3: Global cloud coverage averaged for (a) February and (b) June 2009. White indicates the presence of clouds while blue represents the absence of them. Images from NASA [46].

over the respective month[6]. During each opposing season, northern South America and Southeast Asia appear very cloudy; India does as well, but during the monsoon (June through September).

Using the matrix of Table 1.3 and the cloud-cover images of Figure 1.3, overlap appears for Peru. However, this location does not necessarily represent the ultimate target market since this analysis was quite superficial. Future market studies should be performed before a final target location is selected.

[6] Each pixel was assigned a gradient value between 100% (complete cloud cover) and 0% (no cloud cover) corresponding to white and blue, respectively. Note that the equatorial region is consistently cloudy as this is the Intertropical Convergence Zone where easterly trade winds meet from the Northern and Southern Hemispheres, pushing moist air into the atmosphere where it condenses to forms clouds and rain [46].

Chapter 2

Product Design: Modeling, Laboratory Testing, and Experimental Results

Generally speaking, the design of a product should be done with as much user interaction as possible. This is to ensure that the problem is correctly understood and that the resulting solution is appropriate for the user. However, due to their remote geographic locations, a best-effort prototype was developed without *direct* user interaction. To substitute, numerous interviews were conducted with those having relevant knowledge and suggestions.

This chapter documents the development of this laboratory prototype, which will be referred to as *Kettlectric*. Its thermoelectric module is concealed within a kettle interior to charge an on-board battery which can be detached for powering end-use devices such as a task light or mobile recharger. A high-level representation of the system is shown in Figure 2.1. The Power Generation sub-system consists mainly of the thermoelectric module while Charge and Storage includes a charge controller and re-useable battery. The End-Use sub-system categorizes user devices such as a flashlight, mobile recharger, or radio. Note that Kettlectric was kettle- instead of pot-based to ensure water

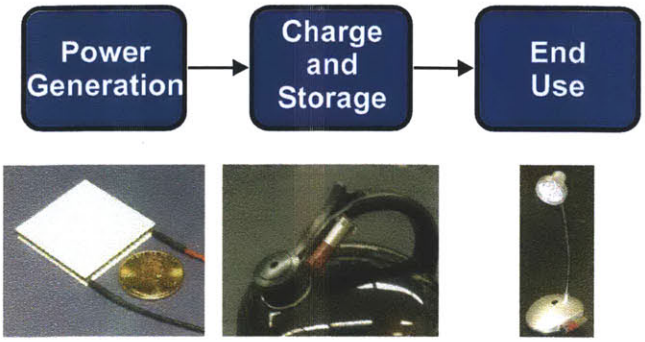

Figure 2.1: A high-level representation of the Kettlectric system. The Power Generation subsystem, consisting mainly of a thermoelectric module, charges the battery through a controller (Charge and Storage) which can then be used to power user devices such as a light, mobile recharger, or radio (End-Use).

placement in the vessel which is required for adequate performance.

2.1 Development and Description of a Simulation Environment

In order to evaluate prototype systems, a controlled and repeatable simulation environment was required that adequately simulated field conditions, the most critical element being the heat source. In Tanzania, for example, over 95% of the population uses solid fuel for energy consumption [47]. Although this estimate does not distinguish between fuel types (e.g. wood, dung, charcoal), field observations suggest wood as most commonly used. Thus, wood fuel was tested for heating characteristics. A gas stove was then selected for approximation to enable repeatable testing conditions.

2.1.1 Flame-Source Modeling

Before quantification of either the wood or gas fuel source, an adequate model was required to describe their heating. This was done by applying lumped-capacitance theory to the heating and cooling of an aluminum cylinder, which was tested in the configuration of Figure 2.2. It was selected for modeling for its straightforward application of lumped-capacitance theory and for its resemblance to a circular cook-pot. During separate trials, it was placed atop a Ghanaian cookstove

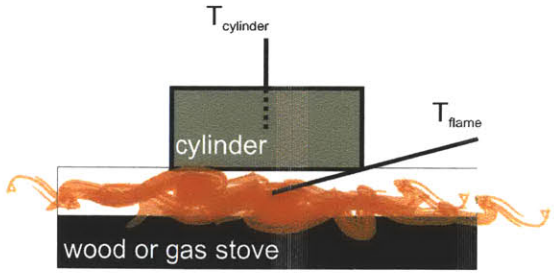

Figure 2.2: The experimental configuration used to quantify heat transfer coefficients for heating and cooling for wood and gas fuels.

and backpacking stove and was heated with the respective fuel: wood and a propane/butane gas mixture. The cylinder was then allowed to cool to room temperature. Throughout each test, the temperature of the cylinder was monitored in the center of its volume, and the flame temperature was measured 5 mm above the fuel plane.

During cooling, the Biot number, Bi, for the cylinder is about 0.003[1]. The hallmark of the capacitance model, as is told by this Bi number, is that resistance to heat transfer lies mainly in the fluid (in this case, the ambient air) and thus allows the solid (the aluminum cylinder) to reach an internal uniform temperature. This makes application of the first law of thermodynamics especially simple. With no mechanical work involved, the first law can be written as

$$\dot{Q} = \rho c V \frac{dT}{dt},$$

where $\dot{Q}$ is the rate of heat transfer into and out of the cylinder, ρ is its density, c is the specific heat capacity, V is the volume, T is the bulk temperature, and t is the time[2]. With Newton's law of cooling, initial conditions, and updated nomenclature ($\theta = T - T_\infty$, where T_∞ is the ambient air temperature), the following expression can be written to describe the cylinder's temperature profile during cooling:

[1]Experimental data taken in a fume hood were used to approximate the heat transfer coefficient used to calculate an initial Bi number. Once it was established that $Bi \ll 1$, a lumped capacitance model was fit for a more precise value of h.

[2]This derivation follows that in Cravalho et al. [48].

$$\frac{\theta}{\theta_i} = e^{\frac{-h_c A_s}{\rho c V} t},$$

where h_c is the cooling heat transfer coefficient and A_s is the surface area exposed for convective losses. Since all other parameters were known, this expression was used to quantify h_c, which was found to be about 11.3 $\frac{W}{m^2 K}$[3]. As is shown in Figure 2.3(a), agreement between the model and experimental data is excellent.

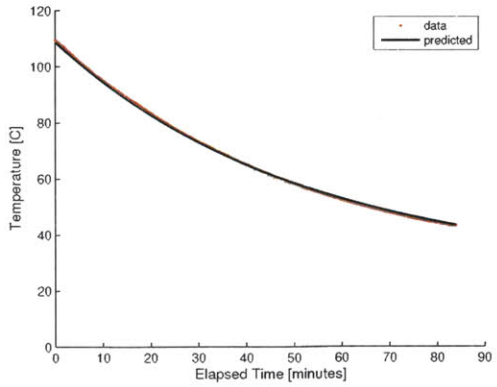

(a) Evidence that the lumped thermal-capacitance model used to predict the cooling heat transfer coefficient is in good agreement with experimental data.

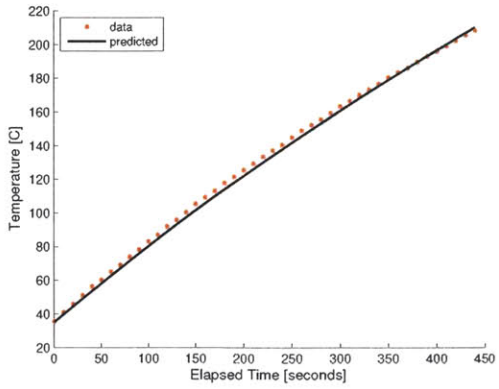

(b) A prediction of the experimental heating profile for an aluminum cylinder over a gas stove.

Figure 2.3: Plots used to verify experimentally measured heating and cooling heat transfer coefficients for an aluminum cylinder.

Once a cooling heat transfer coefficient was quantified, a value for $h_{heating}$ could be obtained. This was done experimentally by heating the same cylinder using a gas and wood flame-source. In this case, the first law appears as:

$$mc_p \frac{dT}{dt} = h_h A_c (T_f - T) - h_c A_s (T - T_\infty),$$

where m, c_p, and T are the mass, specific heat capacity, and temperature of the cylinder, respec-

[3]These data were taken in a laminar-flow fume hood.

tively, h_h and h_c are the heating and cooling transfer coefficients, A_c and A_s the cross-sectional and surface areas of the cylinder, and T_f and T_∞ are the flame and ambient temperatures, respectively. After rearranging, the first law equation can be expressed as

$$\frac{dT}{dt} + aT = b$$

$$a = \frac{h_h A_c + h_c A_s}{mc_p}$$

$$b = \frac{h_h A_c T_f + h_c A_s T_\infty}{mc_p}.$$

The solution of this first-order, linear differential equation is then

$$T = \frac{b}{a} + (T_i - \frac{b}{a})e^{-at},$$

where T_i is the initial cylinder temperature and t is time. This model was used many times to find an average $h_{heating}$ value since all inputs were known. Given the heat transfer coefficient of heating, heat flux was then calculated using experimental temperature data.

An example heating profile for the aluminum cylinder is shown in Figure 2.3(b). Because a time-averaged heat transfer coefficient was used to plot the prediction, the model does not fit exactly. However, the agreement was acceptable so this approach for quantifying $h_{heating}$ was used.

2.1.2 Heating Characterization and Stove Analog Selection

The method for quantifying flame-source characteristics was then used to select the appropriate gas stove analog by comparing its heating to that of wood. The measured profiles for 157 grams of Pine and an isobutane/propane gas mix set to a flow rate of 1.5 grams per minute are shown in Figure 2.4(a). Although the two curves are spaced apart, their profiles, or curve-shapes, are very similar. It

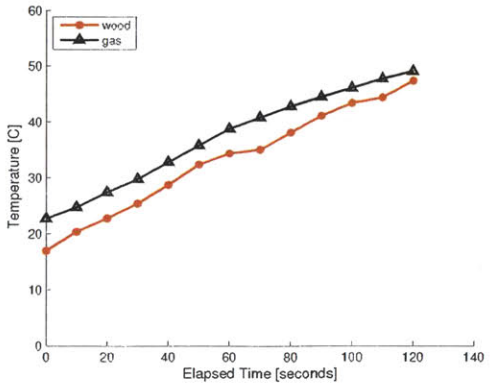

(a) Measured heating profiles of an aluminum cylinder using wood and gas flame sources. Although the gas trajectory is shifted above that for wood, the *profiles* are similar.

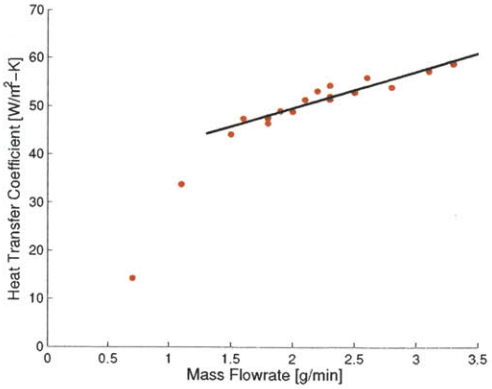

(b) Calibration plot for the gas stove for finding heat transfer coefficient for a given mass-flow setting. Note that the linear fit is only valid above a flow of 1.5 grams per minute.

Figure 2.4: Stove comparison trajectories (a) and prediction plot for $h_{heating}$ from mass flowrate (b).

is clear that a curve shift would place the two trajectories atop one another, which could be done by beginning each test with the same cylinder temperature. In any case, further comparison between heating with wood and gas was made by comparing flame temperature, $h_{heating}$, and average flux. Average flame temperature for the gas stove was 885°C while that for the wood fuel was 707°C; $h_{heating}$ for gas was 33.7 $\frac{W}{m^2K}$ and was 44.4 $\frac{W}{m^2K}$ for wood. These two parameters can be combined by averaging flux, calculated as $q = h_i^{heating}(T_i^{flame} - T_i^{cylinder})$, for each data point i. Despite disagreements in heat transfer coefficient and flame temperature, the fluxes are comparable, with gas being 2.9 $\frac{W}{cm^2}$ and wood at 3.0 $\frac{W}{cm^2}$. The similarity in average flux reinforces the agreement in Figure 2.4(a) and validates the use of a gas stove as an analog for wood[4].

Because the gas stove was capable of simulating the biomass heating, it was further modeled. Specifically, heat transfer coefficient, flame temperature, and average flux was calibrated for given mass flowrates. For example, Figure 2.4(b) allowed for simple identification of heat transfer coefficient based on the stove's flowrate setting[5]. Above about 1.5 grams per minute, the well-fitting linear trend was used to predict the heat transfer coefficient.

[4]Note that thermocouple placement for flame temperature affected tremendously the computation and final value for $h_{heating}$. For consistency, the thermocouple was always located in the same place for each respective flame source.

[5]Flowrate was calculated from the slope of a mass-time plot for the gas canister.

Figures 2.5(a) and 2.5(b) give plots of flame temperature and average flux. The flame temperature

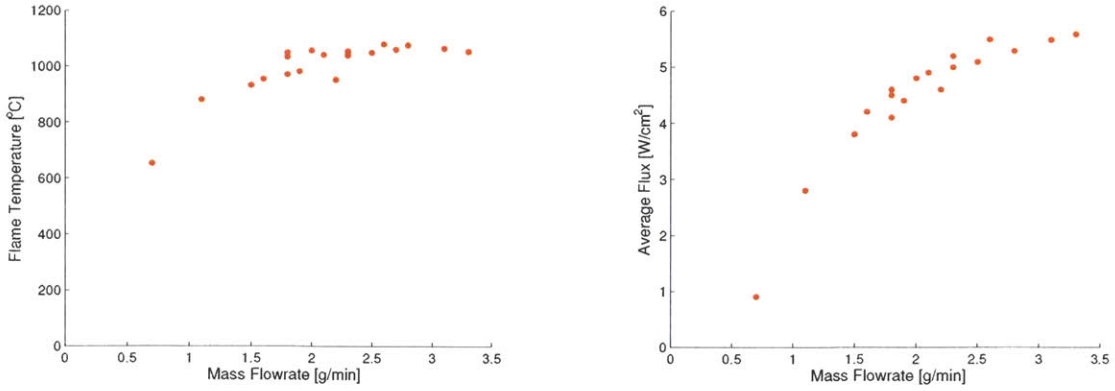

(a) (b)

Figure 2.5: Flame temperature (a) and average flux (b) calibrated for mass flowrate of the gas camping stove.

seemed to settle around 1000°C above about 1.5 grams per minute while the average flux grew rapidly for low flowrates and then more slowly for higher ones.

Maximum Operating Conditions

Although biomass is the main fuel-source in the developing world, gas burning stoves do exist and could be used to heat Kettlectric. Given that the energy content of dry biomass (21 MJ/kg) is far below that of propane (46 MJ/kg, lower-heating value [38]) and kerosene (43 MJ/kg, higher-heating value [49, 50]), the gas stove was used to quantify maximum operating conditions for heating.

Figures 2.4(b), 2.5(a), and 2.5(b) present the maximum-operating information. For each plot, the maximum parameter can be seen at a mass flowrate of about 3.5 grams per minute, which was the highest setting for the gas canister. The maximum heat transfer coefficient was about 60 $\frac{W}{m^2K}$ while the maximum average flux was about 5.5 $\frac{W}{cm^2}$. Figure 2.5(a) shows a maximum temperature of around 1050°C, measured with a thermocouple location of 5 mm from the surface of the burner. In previous tests with variable thermocouple location (data not included in Figure 2.5(a)), the maximum recorded temperature was around 1220°C. Thus, this latter value was used

in all subsequent calculations.

The maximum operating conditions identified here assume *heat transfer by convection.* If the kettle were placed directly on hot coals, for example, heat transfer would occur by conduction and the system would likely overheat. This could be prevented by including an over-temperature alarm to alert the user.

Field-Test Validation

The method of Section 2.1.1 was used to characterize heating from a cooking fire in northern Tanzania during field study in January 2010. The average flame temperature was found to be about 770°C given that the thermocouple probe was inserted directly into the bottom-most layer of hot embers. This 770°C was only about 9% higher than the 707°C recorded during laboratory testing. However, results for heat flux and heat transfer coefficient were different. The time-averaged heat transfer coefficient was measured at 12 $\frac{W}{m^2K}$ while time-averaged heat flux measured only 0.9 $\frac{W}{cm^2}$. These low numbers are due to the cylinder's location, which was far from the heat source in both height and horizontal distance, as is seen in Figure 2.6. The cooling heat transfer coefficient was estimated to be 5 $\frac{W}{m^2K}$ given an ambient temperature of 32°C.

Figure 2.6: Shown in white is the approximate footprint of the test cylinder used to determine heat flux and heat transfer coefficient.

Table 2.1: Limiting factors driving subsequent iterations for the initial Kettlectric prototypes.

Strategy	Limiting Factor
Steam pipe	Temperature differential
Module enclosures	
Full pot bottom	Obstructing heat flow into pot
Box extrusion	Insufficient high temperature resistance
Uniform	Thermal circuit/manufacturability
Castable	Insufficient high temperature resistance, limited bonding

2.2 Power Generation System

With an understanding of the heating environment, the Power Generation system could be developed. The main task was to optimally locate the thermoelectric module such that: a large temperature difference was maintained across it, the high-side temperature was regulated, failure would not occur by dry boil, and it would be fixed mechanically with allowance for thermal expansion. Initial strategies for satisfying these criteria are found in this section and are listed in Table 2.1 for clarity.

2.2.1 The Steam Pipe Approach

The first strategy, termed the "steam-pipe" method, is depicted in Figure 2.7, in which water drips into a heated pipe to vaporize and transfer heat energy to the high-temperature side of the module. During dry-boil, heat would only conduct to the module through the pot and steam pipe since water would no longer be present; the conduction path could then be configured to prevent overheating of the module. Also, by using boiling water as the transfer medium, the high-side would be maintained at a constant temperature regardless of the flame source. Although promising, this method is limited in temperature differential: the maximum ΔT would be about 80°C, assuming the low-side could be brought down to room temperature, which is unlikely.

Many additional ideas were then considered for increasing the temperature differential. The most promising was based on the steam pipe design, but would replace water with a fluid of higher

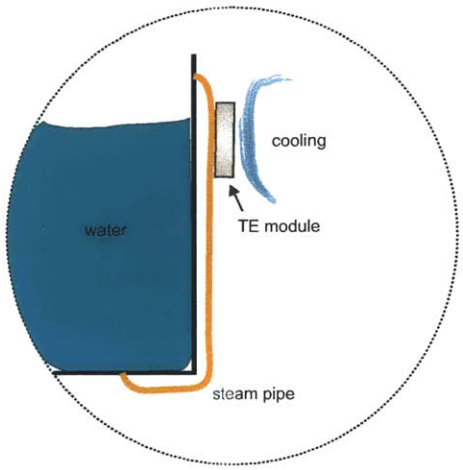

Figure 2.7: Representation of the steam pipe strategy for the Power Generation sub-system. It has many positive attributes but is limited in achievable temperature differential.

boiling point, contained within a closed loop. This would ensure constant temperature during both dry boil and normal operating conditions. However, working with these fluids would be difficult. With a sealed system, excessive heating would pressurize the vessel to a dangerous level. If left open, the fluid may leak. This would pose a problem for sustainability (since the fluid would not be commonly available) and safety, since most of the identified fluids are flammable.

Ultimately, it was decided that damage to the module by dry-boil could be prevented with an over-temperature alarm, so simpler designs for Kettlectric were pursued.

2.2.2 Kettle External Enclosures

The external enclosure method locates the low-temperature side of the module against the bottom exterior of the kettle, and encloses it for mechanical fastening and thermal circuit control. The first iteration is shown in Figure 2.8(a), with the module located in a machined pocket within the aluminum block.

Experimental temperature results are given in Figure 2.8(b), where T_{cold} is the "cold"-side temperature of the module (that which is in contact with the kettle bottom) while T_{hot} represents

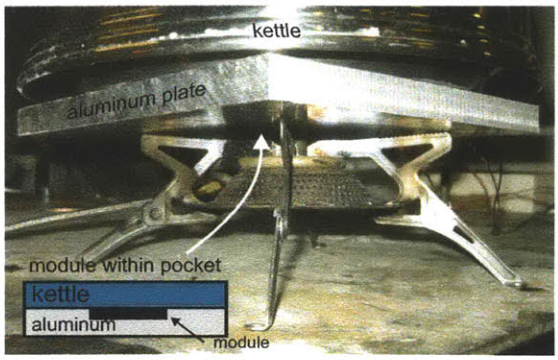

(a) First experimental demonstration of the external enclosure method for locating the thermoelectric module, which sits within a machined pocket in the aluminum plate between the flame source and kettle.

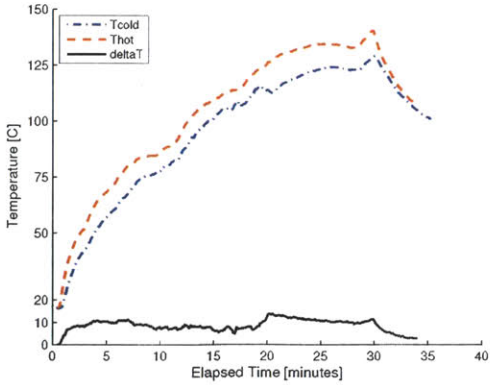

(b) Experimental temperature profiles for the high- and low-temperature sides of the module. The hot side never rose above the maximum operating temperature of the module, but the temperature differntial across it was minimal.

Figure 2.8: Experimental setup (a) and results (b) for the first attempt at locating the generation module between the flame and kettle bottom.

the high temperature side, or that which is in contact with the aluminum plate; "deltaT" is the temperature difference between them. Here, ΔT never becomes much larger than 10°C, and this is for two reasons. First, because of poor thermal interfacing, the cold side of the module is not effectively cooled, as suggested by the high temperatures recorded throughout the test. Secondly, the hot-side temperatures were restricted because much of the heat from the fire was able to flow around the module and into the kettle through the aluminum plate. To increase the module's temperature differential, a new pot-bottom enclosure was developed.

In the new design, depicted in Figure 2.9(a), an insulation material was used to increase ΔT across the device. Given the geometries of the system and the maximum operating conditions tested, the thermal conductivity of the insulator needed to be between 1-3 $\frac{W}{mK}$ to prevent the module from overheating. However, most materials in this range such as ceramics and glass are brittle and difficult to work with [51]. Others were not readily available, were too expensive, or were susceptible to high temperature degradation. It was decided, then, to experiment with organic dirt as it is cheap, readily available, easy to work with, and has a thermal conductivity of about 1.2 $\frac{W}{mK}$ [52]. Surrounding the generator with it would increase thermal resistance of this area thus driving heat flow through the module. In fact, this system was the first to successfully light an LED during

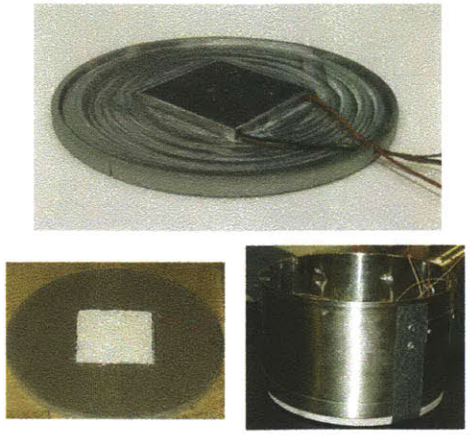

(a) Second iteration to assess the external enclosure method. In this version, insulation was used around the module to drive heat flow through it. Note that a pot was used in place of a kettle for ease of experimentation.

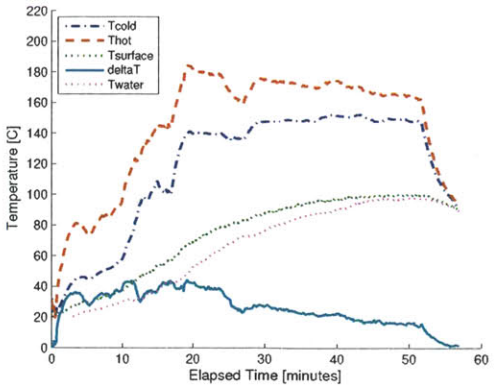

(b) This approach increased the module's temperature differential, but not substantially, due to poor thermal contact on the low-temperature side.

Figure 2.9: Experimental setup (a) and temperature results (b) for the second iteration for the bottom-mounted enclosure.

operation. Although this approach raised the temperature difference to 40°C in some points, with an average in the mid-twenties (Figure 2.9(b)), the improvement was not substantial due to the high temperatures of the cold side. Poor thermal contact to the heat sink caused these large differences. Differential would likely improve with better contact, but this approach is sub-optimal for its use of insulation on the pot bottom, which would increase time-to-boil and fuel consumption.

To negate this effect while still enclosing and protecting the module, a box-extrusion design was constructed. Figure 2.10(a) shows a schematic representation of the approach while Figure 2.10(b) was used to select an insulation material for it. To assemble the system, epoxy was used to bond the thermoelectric module to the pot bottom, as well as the insulation and cap-plate layers; the interface between the plate and box extrusion was sealed with silicone epoxy. Upon testing, the design quickly failed: the silicone by igniting and insulation by bond-breakdown. The system overheated due to high thermal resistances. However, testing demonstrated the success of epoxy-bonding the cold-side of the module, as average temperature differences of less than 2°C were seen between it and the interior pot surface.

To prevent failure due to overheating the thermal circuit was improved. Instead of forcing heat

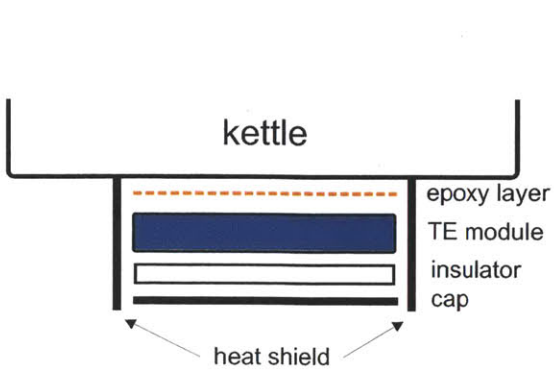

(a) A visual representation of the box extrusion approach. In practice, all horizontal surfaces were in thermal contact.

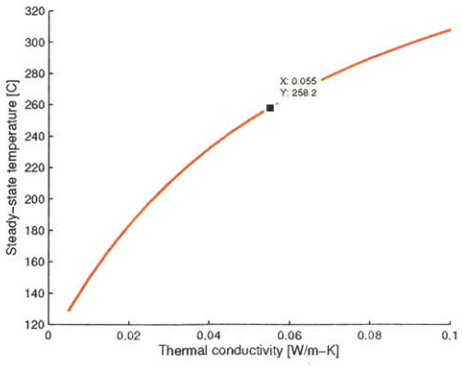

(b) Thermal conductivity selection chart for the insulation material of 5 mm thickness. Steady-state temperature is of the hot side of the module during boiling.

Figure 2.10: The box extrusion design approach which quickly failed during testing.

strictly through the module as in the extrusion design, an alternative heat flow path was introduced by making the enclosure one continuous piece, as is shown in Figure 2.11(a). In this case, heat can

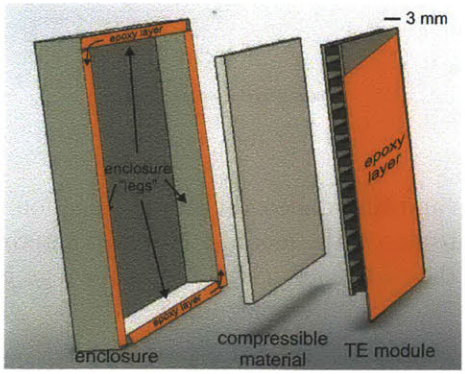

(a)

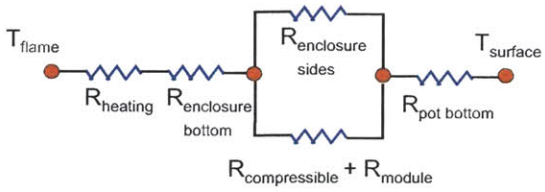

(b)

Figure 2.11: Digital model (a) of the enclosure assembly with compressible material to allow for thermal expansion of the module; the thermal circuit is shown in (b).

flow into the bottom of the enclosure then through the module *or* through the enclosure side walls, or "legs". Compressible material was used between the enclosure and module to allow for thermal expansion in the system.

To design the enclosure and select a compressible material, the thermal circuit of Figure 2.11(b) was modeled in steady state using a heat transfer coefficient of 61 $\frac{W}{m^2K}$, a $T_{surface}$ of 105°C, and

a flame temperature of 1200°C. To prevent thermal short circuit, the enclosure legs were made to have the most resistance possible and thus were modeled of stainless steel with thicknesses of 1.5 mm. With these parameters set, the compressible material's thickness and thermal conductivity could be selected to keep the module's high-side temperature within range during maximum heating conditions.

Figures 2.12(a) and 2.12(b) were used to examine the effects of varying properties for the compressible material[6], which was included in the design for relaxed tolerance requirements and simplified

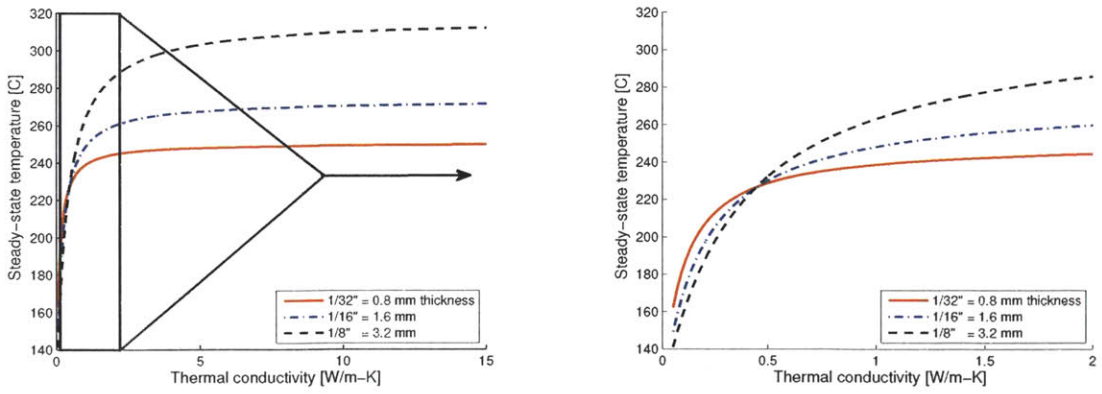

Figure 2.12: Compressible material (of varying thickness and thermal conductivity) selection plots showing steady-state temperature of the high temperature side of the module. Note the interesting crossing behavior in (b) which is due to the fact that the resistance of the enclosure legs grows more quickly than that of the insulation material as the enclosure becomes taller.

assembly, as well as to allow for thermal expansion of the thermoelectric module during operation, which was expected to be on the order of 50 microns[7]. The figures show steady-state hot-side module temperatures against thermal conductivity for different material thicknesses.

Figure 2.12(a) shows rather constant behavior for thermal conductivity values over about 5 $\frac{W}{mK}$, suggesting constant steady-state temperature for any value thereafter. In this regime, the resistance of the compressible material is already much lower than that of the stainless enclosure legs, so decreasing it further would not greatly affect heat flow. Thus, steady-state temperature is tunable

[6]Note that Figure 2.12(b) is simply a "zoomed-in" view of Figure 2.12(a).
[7]Calculated with values from Taylor and Ashby [53, 51].

by material thickness.

This observation does not hold for smaller values of thermal conductivity, however. Figure 2.12(b) shows a cross-over point at about 0.5 $\frac{W}{mK}$. Before this value, a thicker material would give a lower steady-state temperature for a given value of k since it would drive more heat flow through the enclosure legs. On the other hand, after this point, using a thicker material would result in a *higher* steady-state value since its resistance would be lower than that of the enclosure legs which would have correspondingly increased in height to accommodate the thicker material. Faster growth of the leg resistance for low values of k drives this behavior.

For the initial enclosure prototype, high-temperature silicone ($k = 0.3\frac{W}{mK}$) was used as the compressible material. It was clamped between the enclosure and high-temperature side of the module by joining both the low-temperature side of the module and enclosure legs to the pot bottom with epoxy. With a compressible layer of 0.030 inch, the steady-state temperature was measured as 189°C, within 2% of the predicted value. The temperature differential was about 60°C on average with a ΔT of about 80°C for more than half of the test. Increasing the mass flowrate to 2.5 grams per minute brought the steady-state high-side temperature to about 300°C, giving a differential of about 200°C. However, this heating environment caused the system to fail. Force from thermal expansion of the silicone material, coupled with intense heat broke the epoxy bond between the enclosure legs and pot bottom. The complete system, both before and after assembly, is shown in Figures 2.13(a) and 2.13(b).

The design of this enclosure puts challenging constraints on the thermal circuit. In order to achieve an acceptable high-side temperature, the resistance of the enclosure legs must be increased accordingly. Even with low-conductivity stainless steel, the legs must be very thin, to the point where machining becomes extremely difficult. To allow for an enclosure with thicker legs, materials of even lower thermal conductivity were sought.

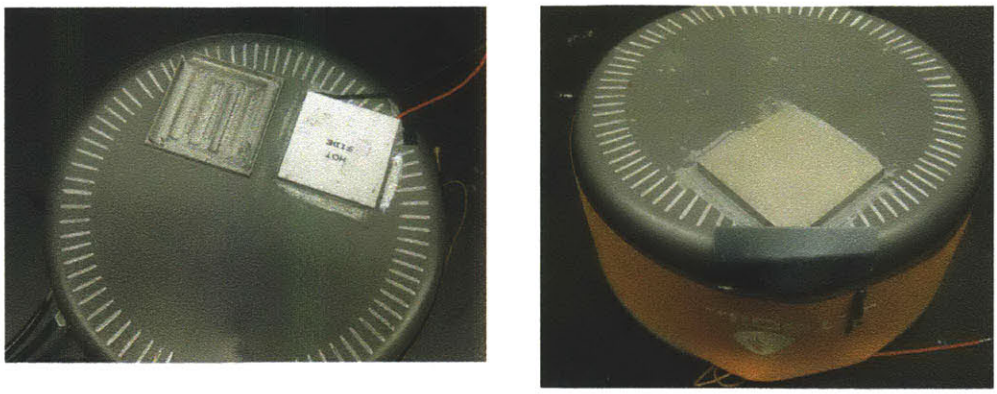

(a) (b)

Figure 2.13: (a) Stainless steel enclosure and bonded module prior to assembly. (b) The fully assembled system including a heat shield to protect the module's output wires from damage.

Table 2.2: Cotronics [54] castable materials summary in order of descending relevance. Cure temperature is binary for whether the material cures below the maximum operating temperature of the module.

Material	Not Brittle	Bonds	Cure Temp.	Rated Temp. °C	Expansion 10^{-5}/°C	Conductivity W/m-K
954FS	x	x	x	1100	1.8	1.4
4701	x	x	x	315	6.4	1.9
132	x	x	x	260	4.1	5.8
4703	x	x		315	3.9	2.6
989FS	x		x	1650	0.8	2.2
940		weak	x	1100	1.8	1.4
810			x	1650	0.8	2.2
906			x	1650	1.3	5.8
903	unknown	unknown		1790	0.7	5.8

Castable External Enclosures

Castable materials offer low values for thermal conductivity and high-temperature operation while facilitating fabrication of parts. In selecting a material, thermal expansion, thermal conductivity, high temperature tolerance, and resistance to fracture were all considered. Further, the material had to bond to the module's ceramic and the metallic pot-bottom. A list of considered products from Cotronics Corporation [54] is given in Table 2.2. Castable prototype examples are also shown in Figures 2.14(a) and 2.14(b).

The compounds toward the bottom of the list offer extremely high temperature operation, but are brittle and do not bond well to metallic surfaces. On the other hand, those with strong bonds (4701,

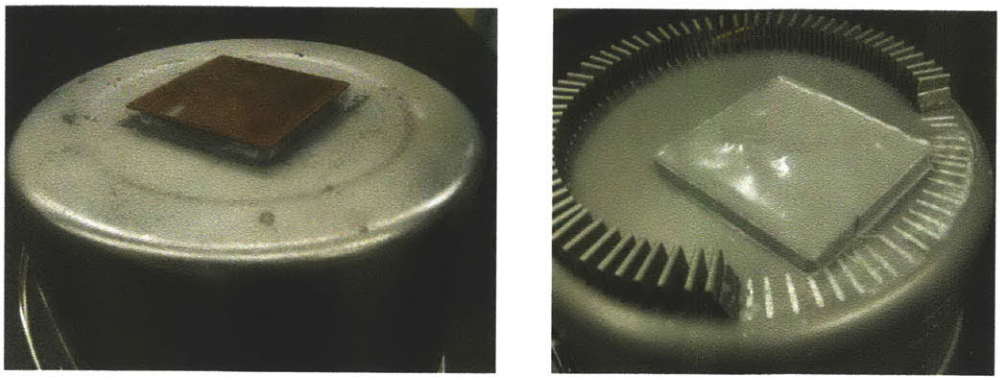

(a) (b)

Figure 2.14: Representative examples of cast prototypes with (a) and without (b) a copper heat spreader.

132, 4703) have much lower rated temperatures. One particular chemistry, 954FS, appeared to offer both advantages, with operation up to 1100°C with strong bonding to metal. It was cast around a bonded module and affixed with a heat spreader to prevent hot spots (similar in appearance to the cast shown in Figure 2.14(a)). Initially promising, the system eventually failed after several cycles of testing, with degradation of the cast-to-pot bond.

A hybrid approach was also attempted. In this case, type 810 was first cast around the module for shaping and was then removed and re-bonded to the pot bottom using 132 epoxy. Although resistant to high temperatures, the surface of the 810 cast began to break down when exposed to open flame. The use of a heat shield such as shown in Figure 2.14(a) helped slightly, but was not easily bonded to the bottom of the cast.

At the outset, castable enclosures seemed promising, but testing showed that these materials could not satisfy all of the design requirements. Thus, a new approach for locating the thermoelectric module was pursued.

2.2.3 Internal Module Clamping: The Water Barrier Method and Kettlectric

With several unsuccessful attempts at locating the module on the exterior of the vessel, this approach was abandoned for a new idea: placing the module on the inside and out of view from the user. Simply locating it against the bottom wall was not enough, however, as the water cools this region effectively, preventing a temperature differential from developing. But if the region around the module is insulated from cooling, the high-temperature side will heat beyond the water's temperature. This is the basic premise of the Water Barrier method.

Figure 2.15(a) graphically depicts this idea. As is shown, the barrier is present to keep water

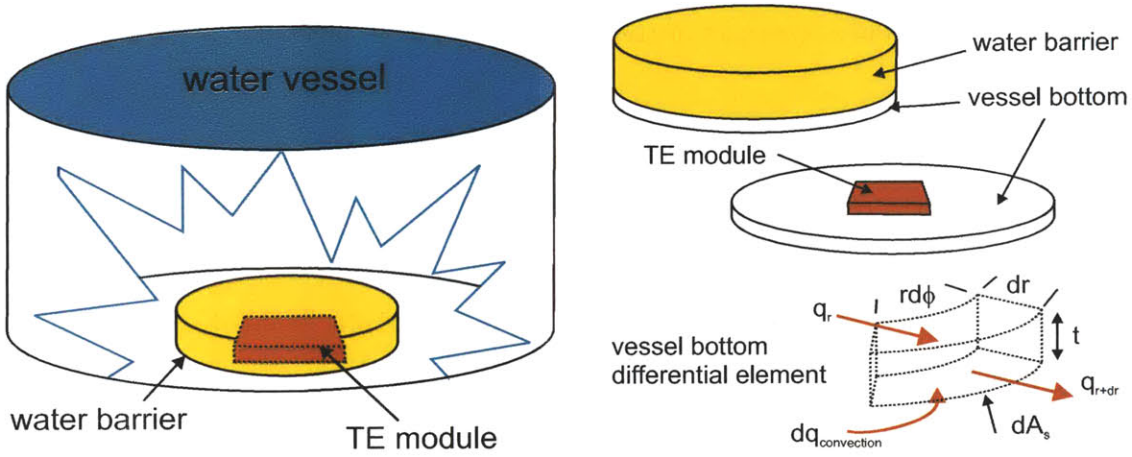

(a) Schematic representation of the water barrier method for isolating the thermoelectric module. In practice, it would be located out of view under the barrier, but would be thermally connected to it so as to transfer heat into the water.

(b) Definitions for deriving the model to predict the temperature profile across the vessel bottom.

Figure 2.15: The design (a) to isolate the module is modeled beginning with the definitions in (b).

from cooling the vessel-bottom "disk" in proximity to the module. Heat that is absorbed must travel a greater distance through the thin-walled bottom, thus allowing temperature elevation at the center of the disk. By adjusting the barrier's radius, the steady-state hot-side temperature can be controlled.

To predict this temperature for different barrier geometries, a model was developed using the definitions of Figure 2.15(b) and the following boundary conditions: the system is in steady state;

the temperature at the outer edge of the disk is that of boiling water, 100°C; the temperature gradient at the center of the disk is zero; the top of the disk is adiabatic; and finally, there is zero temperature gradient across the thickness of the disk.

Referencing Figure 2.15(b), a differential element for the vessel disk is shown with heat flowing radially through the element from r to $r+dr$ and by convection over the differential area dA_s. The thickness of the element is t and it is swept through an angle $d\phi$. In this representation, q is the heat flow, measure in watts. Conservation of energy to the differential control volume demands that

$$q_r + dq_{conv} - q_{r+dr} = 0,$$

where q is heat flow and dq_{conv} is the differential convection to the bottom of the element. Fourier's law, that $q_r = -kA_c\frac{dT}{dr}$, and Newton's Law of Cooling, $dq_{conv} = hdA_s(T_\infty - T)$, can be substituted. The variables k, A_c, h, and T_∞ represent the thermal conductivity, cross-sectional area, flame-source heat transfer coefficient, and the flame-source temperature, respectively. Note that ΔT was written to be positive ($T_\infty > T$) and the term q_{r+dr} can be written as $q_r + \frac{d}{dr}(q_r)dr$. Inserting the latter into the energy equation gives

$$-kA_c\frac{dT}{dr} + hdA_s(T_\infty - T) - [-kA_c\frac{dT}{dr} + \frac{d}{dr}(-kA_c\frac{dT}{dr})dr] = 0,$$

and simplification yields

$$A_c\frac{d^2T}{dr^2} + \frac{dA_c}{dr}\frac{dT}{dr} + \frac{h}{k}\frac{dA_s}{dr}(T_\infty - T) = 0.$$

By using the general formula for the area of a circular section, $A = \frac{1}{2}r^2\theta$, the differential surface area of the element can be found as $rdrd\phi$ if the dr^2 term is dropped; this implies that $\frac{dA_s}{dr} = rd\phi$. The cross sectional area can be found easily, and is $trd\phi$ giving $\frac{dA_c}{dr} = td\phi$. Substitution and simplification gives

$$\frac{d^2T}{dr^2} + \frac{1}{r}\frac{dT}{dr} + \frac{h}{tk}(T_\infty - T) = 0.$$

Following Mills [55], let $\beta^2 = \frac{h}{tk}$, $z = \beta r$, and $\theta = \frac{T-T_\infty}{T_e-T_\infty}$, where T_e is the temperature at the

perimeter of the disk. The equation now appears as

$$r^2\frac{d^2T}{dr^2} + r\frac{dT}{dr} - \beta^2 r^2(T - T_\infty) = 0$$

or

$$z^2\frac{d^2\theta}{dz^2} + z\frac{d\theta}{dz} - z^2\theta = 0.$$

This is the 0^{th} order modified Bessel equation with solution $\theta = C_1 I_o(z) + C_2 K_o(z)$ where C_1 and C_2 are constants, I_o is the zero order modified Bessel function of the first kind, and K_o is the zero order modified Bessel function of the second kind. At $r = r_1 = 0$, $\frac{dT}{dr} = 0$ which means that at $z_1 = \beta r_1$, $\frac{d\theta}{dz} = 0$. Similarly, at $r = r_2$, $T = T_e$ meaning that at $z_2 = \beta r_2$, $\theta = 1$. Using the boundary conditions, the solutions appears as

$$\theta = C_1 I_o(z) + C_2 K_o(z),$$

where

$$C_1 = \frac{K_1(z_1)}{F(z_1, z_2)},$$

$$C_2 = \frac{I_1(z_2)}{F(z_1, z_2)},$$

and

$$F(z_1, z_2) = I_o(z_2)K_1(z_1) + I_1(z_1)K_o(z_2).$$

I_1 and K_1 are the first order modified Bessel functions of the first and second kind, respectively.

An example temperature profile across the radius of a disk is provided in Figure 2.16(a). As is expected, the maximum temperature occurs at the center of the disk and then falls off to the boiling temperature at the disk's outer edge. In Figure 2.16(b), the steady-state temperature of a disk center is plotted against the heat transfer coefficient of heating, and includes experimental data points which agree well with the predictions.

Experimental data were then taken with a thermoeletric module in place. As expected, Figure

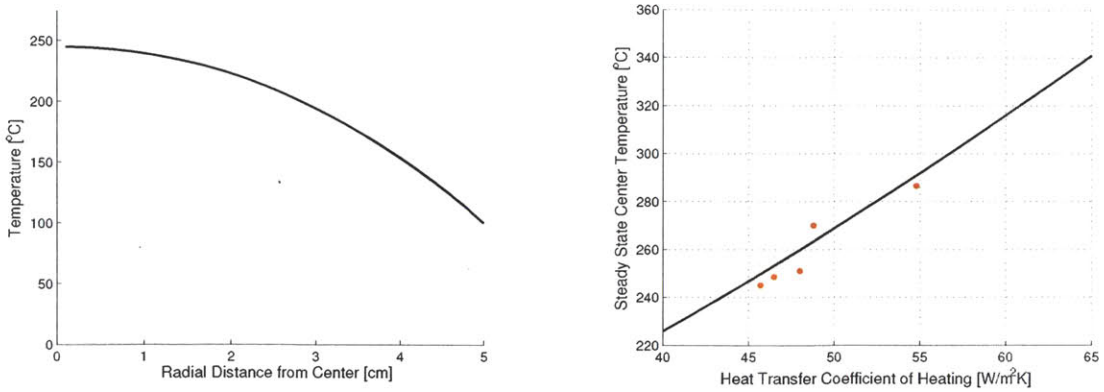

(a) (b)

Figure 2.16: The theoretical model predicts temperature profiles during steady-state similar to that shown in (a). (b) Experimental data for temperature and $h_{heating}$ were collected to verify the model.

2.17 shows values for the steady-state center temperature below those predicted by the model[8]. However, most all recorded points fell within an 85% band of the prediction, a useful observation

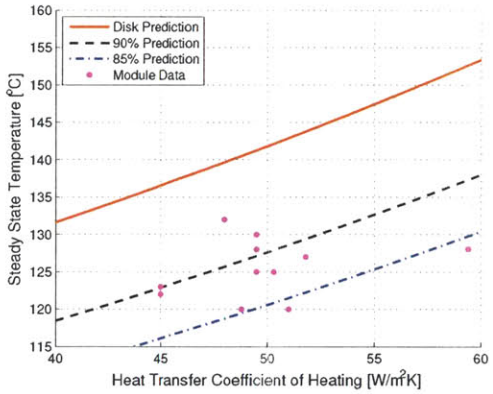

Figure 2.17: Although not accounting for the presence of a module, the disk model can be used to make steady-state predictions to within about 15% of the measured temperature values.

that was used for future system design. This somewhat crude model provided enough information to develop initial prototypes, with the first shown in Figure 2.18(b) with a water barrier diameter of 9 cm.

Apart from barrier geometry selection, methods for module fixation were developed. Functional

[8]Recall that the model did not include the presence of the module. With it in place, it offers an additional path for heat conduction, thus lowering the disk temperature.

requirements included keeping the module in place, allowing for thermal expansion, and creating superb thermal contact. The use of epoxy was first evaluated following the schematic in Figure 2.18(a). By bonding the module to the kettle, thermal contact would be maintained even with

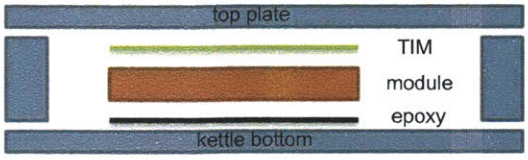

(a)

(b)

Figure 2.18: A schematic representation of the epoxy method (a) along with a prototype version (b). In (b), (red) food-safe sealant is used to seal the aluminum enclosure from water.

downward pressure on the thin kettle bottom. Thermal interface material (TIM) could then be used on the cold side to maintain pressure across the module even with bowing of the top plate.

Before assembly, however, several epoxies from Cotronics Corporation [54] (954FS, 989FS, 940FS, 906, and 4701) were tested for bonding ceramic and aluminum[9]. Despite sandblasting for roughened surfaces, mechanical clamping, and close attention to each cure cycle, most bonds failed under moderate impact loads (the assembly was simply dropped from waist-height to the floor, simulating a dropped kettle in the field). However, the 4701-type remained intact with dropping and was thus used to assemble the system, which is shown in Figure 2.18(b). Once assembled, the entire water barrier was sealed using RTV sealant. However, leakage of the water barrier during testing prevented a temperature differential from developing.

Instead of attempting to salvage the prototype, the question was asked: Should epoxy and thermal interface material be used at all? Is this the best way to achieve excellent thermal interfaces? In

[9]Note that this round of epoxy testing differed from the previous since a thin layer was used to join two flat surfaces, as opposed to creating a cast enclosure over a module.

short, no. Although epoxy creates little thermal resistance initially, it can break down over time, which is caused by thermal expansion mismatch at the bond interface leading to localized stresses. With repeated cycling, the bond degrades over time and at the very least, thermal conductivity suffers[10]. Secondly, the TIM material creates unnecessary thermal resistance. Given its compressibility and relatively high thermal conductivity, it is extremely useful for certain applications, but there were other designs for Kettlectric that did not require its presence.

One such design, shown in Figure 2.19, used stiff clamping plates and o-rings/silicone sealant to allow for thermal expansion. As is shown, the stiff top and bottom plates clamp the module tightly allowing for excellent thermal contact while the o-rings and sealant prevent water from entering the barrier and allow for thermal expansion due to their compliant nature.

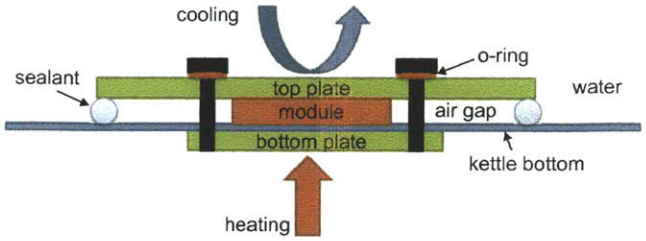

Figure 2.19: A schematic representation of the water barrier design. The stiff clamping plates allow for good thermal interfaces while the o-rings and silicone sealant both prevent water from entering the barrier and allow for thermal expansion.

To select plate thicknesses to prevent "lifting" while clamping, simulations were conducted on aluminum (for its light weight and high thermal conductivity) using Abaqus/CAE. It was found that 1/8 inch thicknesses were sufficient for both the top and bottom plates given the predicted loading conditions[11]. Example deformation contours are given in Figures 2.20(a) and 2.20(b) for 3/32 and 1/8 inch plates, respectively.

With all system components selected, the first Kettlectric system was built and is shown in Figure 2.21(a). The Chefmate^{TM} kettle was specifically selected as the vessel platform since it is not open at

[10] A typical epoxy material expands like 64 $x10^{-6}$ per °C [54] whereas the adjoining ceramic and aluminum expand at 6.5 $x10^{-6}$ per °C and 23 $x10^{-6}$ per °C respectively [35], which span an order of magnitude difference.

[11] For each case, 1025 N of loading (as suggested by Custom Thermoelectric [35]) was applied at each bolt hole of diameter 3.5 mm, which were located 3.5 mm away from the 20 x 20 mm module edges. Reaction forces at the outer diameter of the top plate were not included as it would only be in contact with the compressible silicone sealant in the real system.

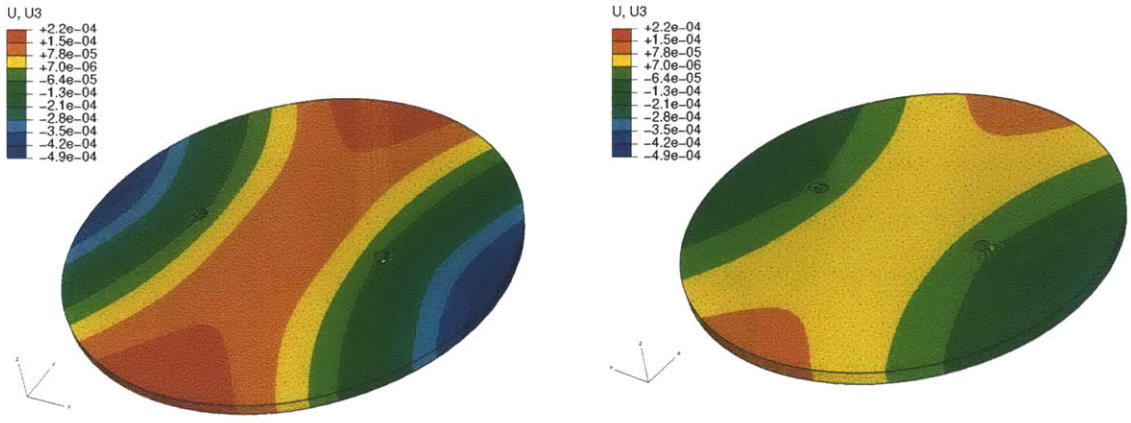

(a) (b)

Figure 2.20: Modeling of the clamping cap to determine required thickness to prevent bowing; (a) shows a 3/32 inch thickness and (b) shows a 1/8 piece. Dimensions are in meters.

the top, thus concealing the water barrier from the user. More importantly, the interior of the kettle was accessible, allowing for assembly of the system (Figure 2.21(b)). The thermoelectric power generator used was a 40 x 40 mm module from Custom Thermoelectric [35] (internal resistance 3 Ω).

Test results of this prototype are shown in 2.22(a) and 2.22(b). The mass flow rate of the test stove was set to 3.4 grams per minute corresponding to a heat transfer coefficient of about 60 $\frac{W}{m^2K}$. The steady-state temperature reached about 235°C, which was predicted by the model as 265°C, a difference of about 13%. Note that this discrepancy falls within 15% of the model prediction (Figure 2.17). The power output peaked at roughly 1.8 W while connected to a simple load consisting of a 4.8 Ohm resistor. Table 2.3 shows further electrical output results, giving steady-state averages for current and voltage.

Referencing Figure 2.22(b), note that the current and voltage exhibit a trend of ramping to a peak followed by gradual decay. This is due to the fact that the impedances of the load and module are not matched throughout, since the module's internal resistance is a function of temperature and that of the load is static. At the peak point, these resistances are most closely matched thus giving the largest power output. Power point tracking (PPT) [31] could potentially be used in the future

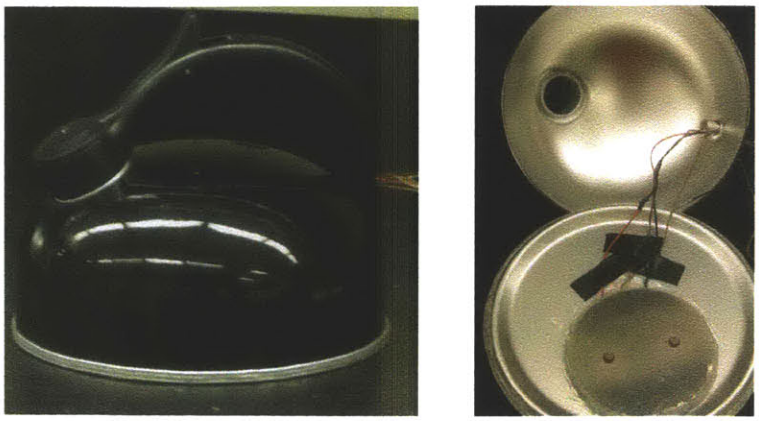

(a) (b)

Figure 2.21: The full assembly (a) and interior (b) of the first Kettlectric system.

Table 2.3: Summarized experimental data for the first Chefmate^{TM} prototype. The model estimate was taken as 85% of the disk prediction while current and voltage were averaged after reaching their respective maximums.

Mass Flowrate g/min	$h_{heating}$ W/m^2K	T_{high}^{actual} °C	$T_{high}^{85\%model}$ °C	Current mA	Voltage V	Power W
3.4	60.0	235	225	515	2.4	1.2
2.4	52.6	200	205	458	2.2	1.0
1.7	47.2	174	187	349	1.6	0.6

to dynamically match impedances between the load and module for optimized electrical output.

The final version of Kettlectric is shown in Figure 2.23(a). Here, a battery clip was installed and wiring was neatly concealed in the handle. Also, all thermocouples were removed, allowing for improved thermal interfaces on either side of the module. With a flow rate of 3.7 grams per minute (corresponding to a heat transfer coefficient of about 62 $\frac{W}{m^2K}$) output reached, on average, about 1.4 W (800 mA at 1.7 V), as is shown in Figure 2.23(b). This is just below the 1.5 W defined in the Product Specifications of Table 1.2. Note that one liter of water was boiled in only 4.5 minutes, providing limited opportunity for generation. A use model should be identified to increase the amount of time for Kettlectric heating. One option would be to encourage users to place it over the fire as it burns out after cooking, a habit practiced by the Maasai of Kenya and Tanzania.

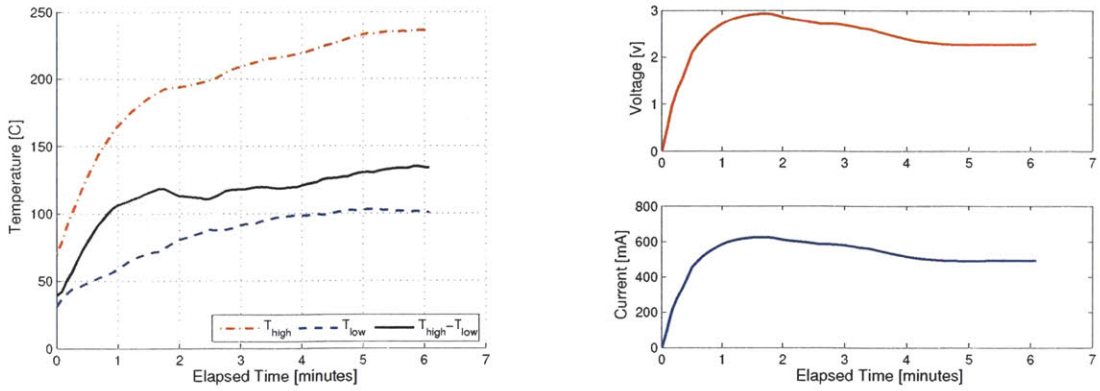

(a) (b)

Figure 2.22: Temperature profiles (a) and electrical output (b) for the Chefmate^{TM} prototype with a mass flowrate of fuel of 3.4 g/min corresponding to a heat transfer coefficient of about 60 $\frac{W}{m^2K}$.

2.3 Selecting a Thermoelectric Module

The Kettlectric system was configured with a promising thermoelectric module from Custom Thermoelectric [35] but was done so without a rigorous selection process. This section will consider module selection more closely to identify an optimal device for use with Kettlectric and future systems.

In selecting a thermoelectric module, the primary optimization parameter is power output to cost, which is given for several power generation modules in Table 2.4. The table was generated from manufacturer data sheets, which provide maximum power output for a given temperature differential. Although the temperature ranges varied, the power ratings listed in the table all correspond to a temperature differential of 200°C.

Looking purely at the power to cost ratio, modules TG 12-8-01L and TG 12-4-01L from Marlow look most promising. However, Marlow's modules are limited in maximum operating temperature, only capable of sustaining 200°C. For this application, this would provide a 100°C temperature differential at most, since the steady-state low-side temperature will be at the boiling point of water. Although many of the modules are capable of significant power output, nearly all are limited by

(a)

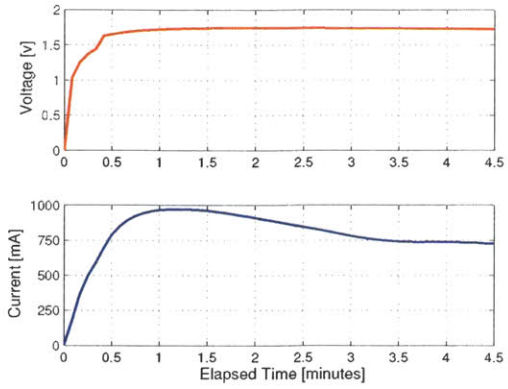

(b)

Figure 2.23: The final version of Kettlectric (a) with the side-mounted battery holder and integrated charge controller. Power output is also given (b) for a flowrate of 3.7 grams per minute corresponding to a heat transfer coefficient of 62 $\frac{W}{m^2K}$.

maximum temperature and thus will never achieve their output potential. The only module that far surpasses the others in this category is that from Thermonamic, with continuous operation at up to 320°C. With it's capacity for highest temperature differential, this module was selected as the optimal device from the pool of candidates given.

To quantify the module's output at its upper operating range, it was heated over a gas stove while cooled with water, thus simulating the heat transfer mechanisms of the Kettlectric system. The resulting output given a gas flowrate of 1.4 grams/minute (corresponding to a heat transfer coefficient of about 45 $\frac{W}{m^2K}$ and flux[12] of about 4 $\frac{W}{cm^2}$) are shown in Figures 2.24(a) and 2.24(b). As can be seen in Figure 2.24(b), the temperature differential was excellent at about 200°C for most of the test. This corresponds to an equally impressive power output throughout, with a maximum of 3.5 W. Note that at about minute 1 of the test, the current logger became saturated and was subsequently disconnected at minute 2, resulting in a gap in the current data and a spike in the voltage trend. Manual current logging resumed at about three minutes at thirty-second intervals. These output results are promising, especially given the module's capacity for continuous operation to 320°C, a 7% increase in high-side temperature.

[12]Note that 110 watts flowed through the module during the test, which was calculated from experimental temperature measurements.

Table 2.4: Power to cost ratios for high temperature power generation modules from four of the major manufacturers: Custom Thermoelectric (Custom T.E.), Marlow Industries Inc., Thermonamic Electronics Corp., and Tellurex.

Manufacturer	Module	Size mm	Cost[a] $	Max Power W	Max Op. Temp. °C	Power to Cost[b] 100*W/$
Custom T.E. [35]	1261G-7L31-04CQ	40 x 40	53	6.2	260	11.7
Marlow [37]	TG 12-4-01L	34 x 30	25	4	200	16.0
	TG 12-6-01L	45 x 40	39	6	200	15.4
	TG 12-8-01L	45 x 40	49	8	200	16.3
	TG 12-2.5-01L	34 x 30	42	2.6	200	6.2
Thermonamic [19]	TEP1-1264-1.5	40 x 40	40[c]	5.9	320	14.8
Tellurex [36]	G2-30-0313	30 x 30	35	1.3	260	7.0
	G2-35-0315	35 x 35	44	1.5	260	7.0
	G2-40-0313	40 x 40	44	1.3	260	6.0
	G2-40-0329	40 x 40	42	2.9	260	14.0

[a] Cost for one module, with no volume discount.
[b] Given a temperature differential of 200°C.
[c] This is the cost per module for an order size of three.

Although the Thermonamic module demonstrated promising results, its cost was still rather high, at $40 per module for a twenty module order. In an attempt to decrease system cost as much as possible, Peltier coolers were considered for potential inclusion since they are generally cheaper. These devices are very similar to power generation modules except in their lower-temperature solder. They are designed to cool objects when connected to an electrical power supply. However, like power generation modules, they can operate reversibly and are thus capable of generating electricity when heat is pumped through them.

However, maximum operating temperature limits their use for power generation. Coolers are generally rated to only about 150-200°C [30], giving a 100°C temperature differential at best. Further, they are design to operate with maximum efficiency at lower temperature differences, whereas generators operate best at relatively higher ones [30]. Thus, Peltier cooling modules did not appear to be appropriate for this application.

To verify, a cooling module from Custom Thermoelectric [35] (not shown in Table 2.4) was tested, but as expected, with limited success. Due to its low temperature rating, the soldered wire leads became detached during heating due to excessive temperature exposure. Even if the device had

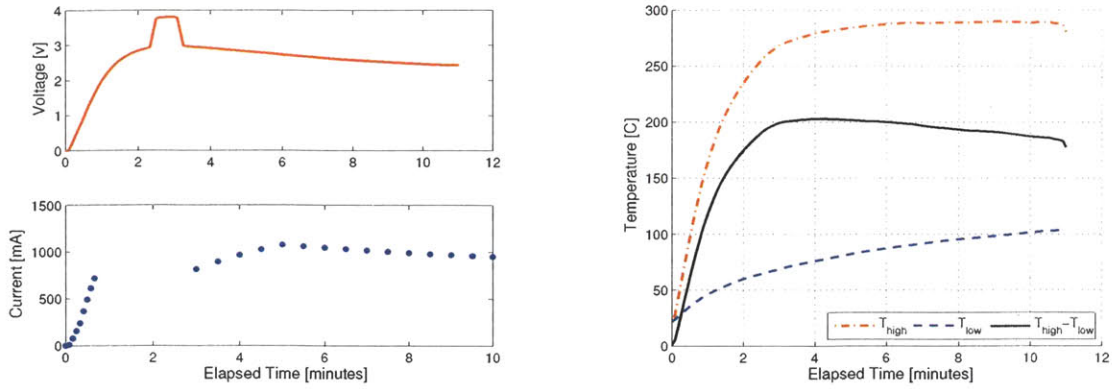

(a) (b)

Figure 2.24: Electrical output (a) of the 40 x 40 mm Thermonamic module given the temperature differential shown in (b). At about 1 minute, the current logger became saturated but was disconnected at about 2 minutes, causing the voltage to spike. Subsequent data points were manually recorded at thirty-second intervals.

remained intact by reducing the high-side temperature, output would likely drop to an insufficient level.

2.4 Charge Control and Storage System

The thermoelectric module of the Kettlectric system will be connected directly to the Charge Control and Storage system, which consists of a charge controller to regulate current and voltage to the battery (while also offering charge termination), and a rechargeable battery which clips into the Kettle's handle. This section further details these components and presents testing and prototyping work completed.

2.4.1 Storage Devices

Various devises were evaluated for storage of the energy flowing from the thermoelectric module. Supercapacitors were first considered for their ability to re-charge rapidly. Given a module output of 2.6 W, fifteen minutes of generation time requires 2.3 kJ of energy storage which is equal to

$\frac{1}{2}CV^2$ for a capacitor. This requires an equivalent capacitance of 250 F if the voltage is brought down to 4 V. A supercapacitor of this size costs about $50 [33], whereas using multiple capacitors in parallel is even more expensive.

A more affordable storage medium is the rechargeable battery. Specifications for selection include total storage, charge rate, cost, lifetime, temperature stability, volume, and weight. Of the chemistries currently available, the NiCAD was selected for initial use in the Kettlectric system given its long life, high charge rate, and economical price [56]. However, the cadmium present is toxic and environmentally damaging, so NiMH technology was also considered. In the end, two battery candidates of each type were identified: A NiCAD AA cell from Sanyo [57] (p/n KR-900AAEC) with a maximum charge current of 1350 mA and storage of 900 mAh, and a NiMH AA from RadioShack (p/n 23-525) [58] with a maximum charge current of 4000 mA and storage of 1800 mAh. As the NiMH is more environmentally friendly and handles higher charge current and storage, this cell was selected for Kettlectric.

2.4.2 Charge Control Circuitry

As important as battery selection was charge-control, which is the dynamic adjustment of current and voltage to the battery, as well as charge termination to preserve battery life and prevent catastrophic failure (e.g. catching fire). Figure 2.25(a) shows the first breadboard prototype of a quick-charge controller. The design allows for three charge rates, gives charge-status indications, and provides regulation and termination. Upon testing with a thermoelectric module, however, it was immediately clear that the controller's impedance was not well matched. Because its resistance was much larger than that of the module, current flow was extremely low and the voltage output too high.

To better match impedance while simultaneously reducing controller cost and complexity, the "charge controller" of Figure 2.25(b) was constructed. With a single diode linking the module to battery, the voltage across the battery was within its tolerable range (1.1 to 1.9 V), current flow was

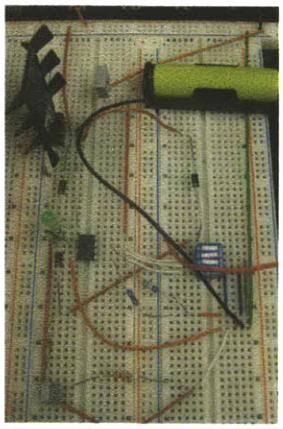

(a) Initial breadboard prototype of the charge controller. This quick-charge design moderates current and voltage to the battery, charge terminates, and is capable of charging at two rates.

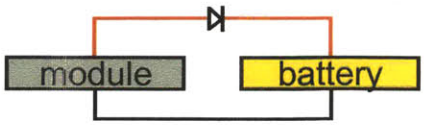

(b) A much simpler "charge controller" consisting of nothing more than a diode. With improved impedance matching, current is increased and the voltage seen by the battery is within its acceptable range. The diode also prevents the battery from discharging and the circuit self-terminates when the battery is fully charged.

Figure 2.25: The complicated breadboard charger of (a) was reduced to the single diode of (b).

maximized, and the battery was prevented from discharging during standby. Furthermore, charge termination was inherent to the circuit since current will tend toward zero as the battery voltage approaches that of the module. This "natural" termination was experimentally verified and results are shown in Figure 2.26(a).

In practice, charge termination for this configuration would occur as the battery voltage climbs to reach the output voltage of the module. To simulate this process, the *module* voltage was instead decreased toward that of the battery. Although a different case, the fundamental idea is the same: allowing voltage equilibration. Thus, experimentally, the intensity of the flame was lowered throughout to slowly decrease output voltage over time. As is shown in the figure, the current tends toward zero as the voltages move toward equality. The final current measured was about 10 mA, classified as a "trickle charge" and thus a safe level of current to pass to an already-charged battery.

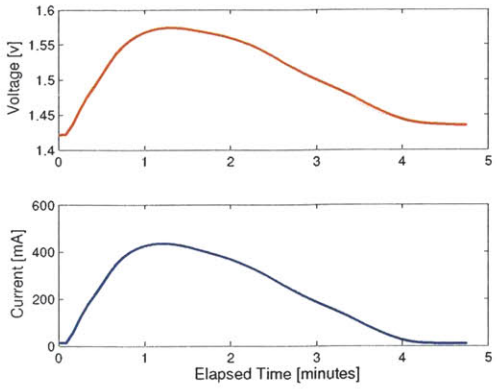

(a) Current and voltage for the thermoelectric module. As the voltage approaches that of the battery (about 1.44 V), current tends toward zero.

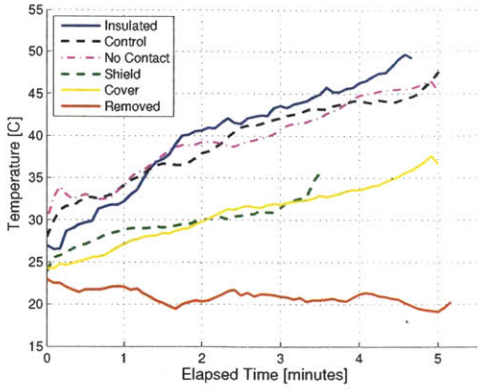

(b) Battery temperature over time under various testing conditions. These results show heating of the battery directly from the flame source and kettle top.

Figure 2.26: A closer look at Kettlectric's battery: (a) inherent charge termination of the diode controller and (b) battery temperature testing during operating conditions.

2.4.3 Battery Safety

The final Kettlectric design locates the battery on the handle of the kettle, which is exposed to heating from the flame-source. Excessive battery heating can cause immediate, catastrophic failure as well as decreased performance over time. To determine whether the battery location was suitable, the Kettlectric system was heated over a flame source with various modifications. The results are shown in Figure 2.26(b). A **Control** test was first conducted in which nothing was done to protect the battery. Further tests were carried out with varying modifications: **Insulated** wrapped insulation material around the battery itself; **No Contact** was preventing the battery from contacting the handle or battery contacts but leaving in the same location; **Shield** was creating a shield to prevent convective heat energy from impinging on the battery; **Cover** was covering the top of the kettle with insulation to prevent radiation and natural convection from the top of the kettle to the battery; **Removed** was remotely connecting the battery to the system to determine whether the high charge current was responsible for increased battery temperature. The results show temperature reductions with Shield and Cover methods, which suggest battery heating by convection from the flame source directly and radiation/convection from the top of the kettle. Wrapping the battery with insulation (Cotronics [54] Ultra-Temp 390 Ceramic Tape, 1/16 inch

thickness) did not have a significant influence on reducing temperature. These results motivate further design to relocated the battery or better shield it from these heat sources.

As discussed above, the diode controller has "built-in" charge termination, but this method is not fail-safe. For example, if the maximum output voltage of the module becomes too great, the equalizing voltage may cause serious damage to the battery. However, if the system is configured to output a safe battery voltage under maximum operating conditions, this may be an acceptable method for charger termination.

2.5 End-Use Applications

Prior to field testing in Tanzania, the main End-Use applications were in lighting and mobile phone recharging, with emphasis on task lighting. Several booster circuits were constructed in order to drive ultra-bright LEDs with the single AA cell of the Kettlectric system.

2.5.1 Lighting

A single AA battery was selected as the storage unit for Kettlectric since it was deemed to have enough capacity for its intended functions. However, this single cell format only provides for about 1.2V of potential, so driving 3 V LEDs for lighting required voltage-boosting circuits. In production, these were expected to be cheaper than adding additional cells to obtain a higher potential.

Figure 2.27(a) shows such a boost circuit, built with an integrated circuit (IC) from Maxim [59], capable of driving LEDs with as little as 0.5 V. This design operated with excellent efficiency, but was expensive, costing $11 excluding the LEDs, breadboard, and battery. Thus, simpler, albeit less efficient boosters, were constructed to decrease cost.

One alternative circuit, shown in Figure 2.27(b), is simple and cheap, with components totaling $1. In basic terms, the circuit works by "charging" the hand-wound inductor until its voltage becomes

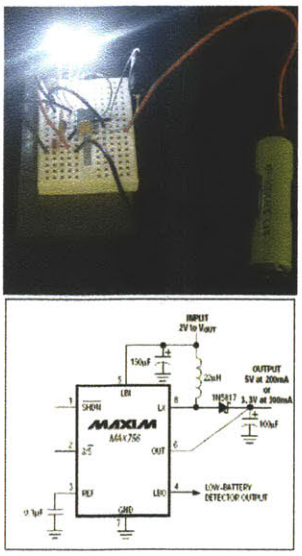

(a) Successful implementation of the integrated circuit design, showing the lighting of three LEDs with a single NiCAD cell. Circuit design from Maxim [59].

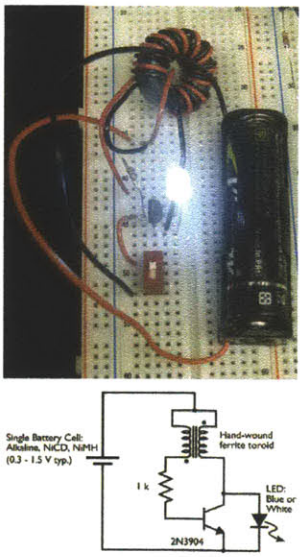

(b) The hand-wound toroid design successfully lighting an LED. Circuit adapted from Make Magazine [60].

Figure 2.27: Voltage boost circuits capable of driving 3 V LEDs with a single NiCAD cell.

large enough to drive current through the LED. The transistor switches on and off to charge and discharge the inductor and the LED correspondingly flickers. It does not appear to blink, however, since the oscillations occur at tens of kilohertz, giving the appearance that the LEDs are always lit.

Two additional circuits were built to improve efficiency of the low cost circuit (Figure 2.27(b)) and are shown in Figures 2.28(a) and 2.28(b). The principle for functionality was the same, i.e. "charging" the transformer to boost voltage until the transistor switched to force current through the LED. Although functional, performance of these circuits was far inferior to that of the IC-based design so despite its added cost, it was selected to drive a task light for use with the Kettlectric prototype.

The IC approach was then taken from the breadboard-stage and was mounted in a perforated board for a sleeker form. Figure 2.29 shows the board inside of the base of the task light which can be concealed to power 14 bright LEDs.

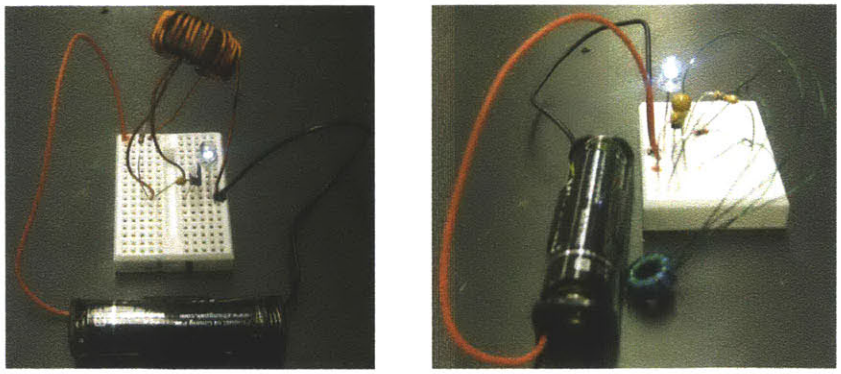

(a) (b)

Figure 2.28: Two improved driver designs to increase efficiency. These are lower cost but do not perform as well as the integrated circuit driver in Figure 2.27(a). Circuit (a) was adapted from Colin Mitchell [61] while (b) is from [62].

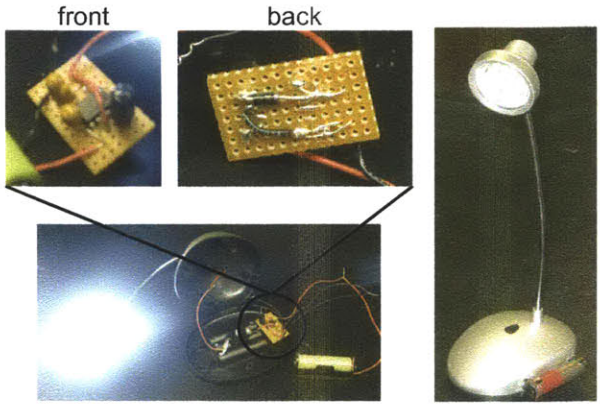

Figure 2.29: The IC LED driver circuit is permanently mounted to a perforated board and inserted into the base of the 14 LED task light.

Assuming a power output of 1.5 W from the Kettlectric system and perfect electronic efficiencies, thirty minutes of charging would provide about 45 minutes of lighting with the 14 LED task light in Figure 2.29. However, if the LED count was reduced to seven (which still provides adequate task lighting), a thirty-minute charge would provide 1.5 hours of lighting.

2.5.2 Mobile Phone Charging

The Kettlectric system could also be the basis for a mobile recharging system where the battery is removed from the handle and placed in a separate mobile recharger. These are available at low cost

and can be operated with a single AA cell. Again, assuming 1.5 W of power output with perfect electrical efficiency, a thirty-minute charge would provide 45 minutes of talk time, given a mobile draw of about 1 W (275 mA at 3.7V) [63]. With about 3 mA [63] of draw during standby time, an additional thirty-minute charge could power the phone for over 60 hours. This would allow users to keep their phones on throughout the day, preventing them from missing important calls from relatives or those regarding job opportunities, crop prices, news events, etc.

Chapter 3

Field Testing and Product Re-Design

Field testing and information gathering was conducted in northern Tanzania during January 2010. Although not selected as a target market in Section 1.3, it was chosen for field study due to the field contacts based there. The purposes of the trip were to test the Kettlectric prototype, further understand customers needs, establish price-points, and understand distribution. While in the field, a major design change occurred, a new business model was developed, price-points were established, and competition was assessed. Additionally, a potential target market was identified, community partnerships were established, and preliminary marketing and distribution plans were discussed. Rural Tanzanians were excited about the idea with one school teacher commenting: "It would be better if I could get it now, right now." However, this man was referring to the *service* offered by Kettlectric and not the product itself. It was found that the use-model for Kettlectric was not in line with Tanzanian cooking habits.

Partners established during the trip include East African Voyage, The Indigenous Education Foundation of Tanzania, and Global Cycle Solutions. The former two, a tour-guide organization and school, respectively, provided knowledge of and intimate contact with local Maasai of all ages; the latter is a for-profit enterprise selling bicycle attachments to improve agricultural productivity. This group has relevant knowledge regarding importation and distribution in Tanzania.

3.1 An Improved Customer Understanding

In visiting local houses in Tanzania, with most belonging to Maasai tribesman, it was immediately clear that Kettlectric was in the wrong form for use, for more reasons than one. First, kettles are used differently than in the US where they are used to boil water directly. In rural Tanzania, however, kettles are used as transfer vessels; a typical one is shown in the inset of Figure 3.1(a). If

(a) A common "three-rock" cooking setup with a pot resting on three points of contact. While this pot is in place, there would be no room for Kettlectric. *Inset* A local kettle.

(b) A cooking area of worked stone, forming a rectangular enclosure inside of which firewood burns on the floor; cooking pots rest across the gap.

Figure 3.1: Home cooking configurations for two locations in northern Tanzania. Neither environment is particularly conducive for use with Kettlectric.

tea is to be served, hot water is first boiled in an open pot over the cooking fire. The water is then poured into the kettle where the tea ingredients are added. The kettle is then used for serving into drinking cups and is placed next to the fire to be kept warm. Thus, a Kettlectric-type system would never be exposed directly to a flame. In addition, there is little space for additional vessels over a cooking fire, as is shown in Figure 3.1. If the breakfast or dinner pot were already in place, there would be no room for Kettlectric. Furthermore, convincing a customer to purchase an additional, rather expensive, cooking container would be difficult. And finally, at least in the areas surveyed, water is not boiled frequently for drinking, "maybe once per two weeks." It is done so in large batches to decrease frequency of the task. Thus, it was clear that a new, more appropriate design was required, one that will be detailed in the next section. However, it is interesting to consider

how Kettlectric might change behavior: it is possible that water would be boiled more frequently in order to derive the electrical benefits of the system. This could have an indirect benefit on health, as contaminated water is sterilized through boiling.

Although Kettlectric missed the mark in form, its capability excited the local people. Having the ability to generate power in the privacy of the home was particularly appealing to the Maasai, who were primarily interested in charging cell phones. They also asked about powering radios and flashlights. In principle this is of course possible, but a viable method for doing this has yet to be discovered. One option would be to use Kettlectric to re-charge different types of batteries which could then be inserted into end-use devices. However, this would be a "tough sell" as rechargeable batteries are at least ten times more expensive than throw-aways. Although they would be better-performing and longer-lasting, convincing users to purchase a set of $10 batteries *in addition* to the generation system when compared with a disposable set for $0.75, would be difficult.

In contrast, the rechargeable battery in a cell phone is a sunk cost for the user. Thus, if the system recharged mobiles directly, it would require no onboard storage. As a result, the power output of the module should not exceed the maximum input of the cell battery which justifies the use of a lower-performing and *cheaper* module. Given an optimized system for universal mobile recharging, the user can generate income by charging others' phones in addition to his or her own. Several Maasai warriors (like the one picture in Figure 3.2(a)) were interested in this system for precisely this reason, and it may be attractive for local market vendors like the women selling maize in Figure 3.2(b). Given a $30-$35 price-point and a single-charge cost of $0.25-$0.30, the system can be paid-off in three to four months, with free personal charging and pure profit thereafter.

Assuming the power output of the system can achieve the maximum input of the average cell phone battery, charging should be completed in about an hour, which is competitive with their current alternatives. Off-grid users generally pay someone else to charge their phones, whether by solar power, grid access, or diesel generator. The appeal of a Kettlectric-like system is that it enables the consumer to become an entrepreneur and lowers the entry barrier to tens of dollars instead of the hundreds required for solar or diesel systems.

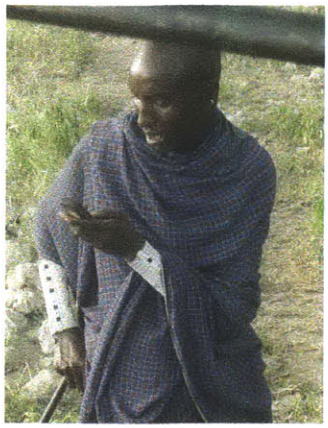

(a)

(b)

Figure 3.2: (a) A Maasai warrior checks his cell phone for messages; in (b), a local woman sells maize along the roadside for income.

Table 3.1: Product specifications based on user feedback and in-country observations.

Customer Need	Product Attribute	Product Specifications		
		metric	*value*	*units*
Competitive Mobile Charging	Complete System	Charge Time	< 1	hour
Pot/Stove Compatibility	Vessel Design	Home Compatibility	> 90	%
Affordability	Complete System	Cost	15-20	$
Value Added	Complete System	Payback Period	< 3	months
Durability	Complete System	Lifetime	7-10	years
Safety	Vessel Interaction	Burn Rate	< 5	%
Ease-of-Use	Complete System	Learning Curve	1-2	hours
Local Reparability	System Components	Fixable Failures	> 90	%

3.2 Abandoning Kettlectric: An Appropriate System

Based on customer feedback from the field, the successor to Kettlectric was designed to be even less disruptive to cooking practices. The idea was to create something that could absorb otherwise wasted heat and send power through insulated wires to a "black box" serving as a mobile or battery recharger. In either case, there would be no on-board storage which would reduce system cost and increase lifetime and safety.

Given the change in design, an updated product contract is given in Table 3.1, with significant changes to the original one, given in Table 1.2. Note that the retail price has come down significantly

from that estimated for Kettlectric, from $30 to $15-$20. This was calculated based on field observations.

On average, it costs about 300 Tanzanian Shillings ($0.23) per mobile charge, and users tend to recharge their phones about two times per week. This accumulates to about $2 of charging expenditures per phone per month. Assuming the system would service two phones, the value for replacing charging expenditures doubles to $4 per month. With a three month payback period, this places the device cost at $12, and assuming that the user would pay for the other advantages of the system, like its convenience (users would no longer need to pay fares to drive into town), for example, willingness to pay might reach $15-$20. This could be increased further for other regions where there are fewer alternatives for charging. This price point seems accurate given the costs of competing technologies in the Arusha area. For example, D.Light's [12] solar lantern and mobile charger combination is priced at $25 yet has been struggling with sales [64]. Finally, notice that the system no longer needs to store energy nor perform as a cooking analog, but must instead be adaptable for all cooking environments.

One way to achieve robustness for any cooking configuration is to extract heat energy from the flame and transfer it to the externally located module via a metal rod; this is depicted in Figure 3.3(a). This allows for the placement of all electronic components away from the fire, which is advantages for safety reasons. However, this idea was quickly dismissed with simple heat transfer calculations. As is shown, driving 50 W of heat power through a 1/4 inch diameter rod over 20 cm requires an extremely large temperature difference, with the upper bound pushing the limits of the material. Furthermore, the addition of this amount of metal would introduce both cost and weight increases.

3.2.1 myGen: A Side-Mount Design

A more plausible design, referred to as myGen is simulated in Figure 3.3(b) in which a module (not visible) is clamped between a plate and water vessel, and the entire device is hooked to the side of

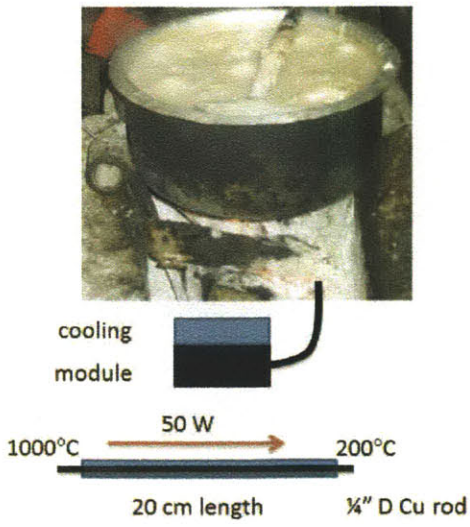

(a)

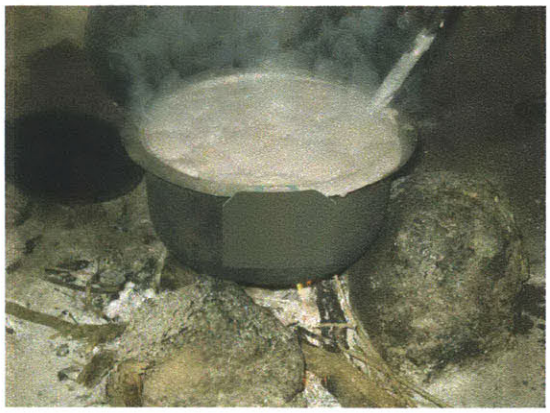

(b)

Figure 3.3: System re-design to extract heat energy more passively by using a copper rod to transmit thermal power to the satellite module (a) or by locating the module beneath a water vessel which clips to the side of a cooking pot (b).

a cooking pot. Convective currents flowing around the pot would impinge upon the bottom plate, transmitting heat through the module and into the cooling water. This side-mount system would require its output wires to be well insulated as they travel from the module to the charging box. In addition to integration with a pot, myGen could be used as a stand-alone device atop a cooking rack, for example.

To begin sizing the system, trial testing was conducted with a 40 x 40 mm Thermonamic [19] power generation module which was clamped between an aluminum plate and a pot, which was filled with water. It was found that a heat flux of 4 $\frac{W}{cm^2}$, corresponding to 110 W of heat power through the module yielded 3.5 W of peak power output with a ΔT of 200°C throughout the test. Based on field-testing, however, heat flux was expected to be 1/4 of this value, so driving 100 W through the module would require 100 cm^2 of heat absorption area. For optimal cooling, on the other hand, water volume should be maximized. But performance was sacrificed to reduce system size, and the resulting vessel and plate, shown in Figure 3.4(a), had a volume of 600 mL and area of 83 cm^2, respectively. Referencing the figure, note that the bottom clamping plate extends beyond the vessel

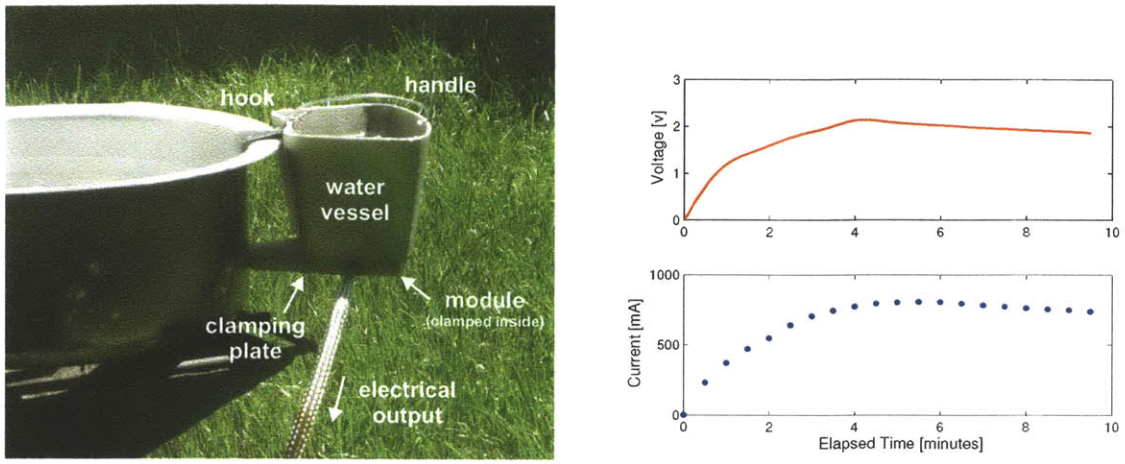

(a) (b)

Figure 3.4: The first myGen prototype in (a) produced the output in (b) when tested under field-simulated conditions.

at the rear to rest against the side of the pot, and the hole at the bottom of the vessel is the exit for the module's wiring, which were protected with Cotronics ceramic-weave wire insulation and a stainless steel sheath. As is shown in Figure 3.4(b), output reached a peak of about 1.8 watts during field-simulated testing. This can be boosted in future versions by increasing the clamping plate area and reducing its contact with the pot to prevent thermal short-circuiting.

To fabricate the myGen system, sand casting was selected for its ability to form sealed, hollow shapes and its accessability in developing countries. Figures 3.5(a) and 3.5(b) describe the process. In the first case, a digital model was used to create a 3D-printed part (Figure 3.5(a)), which was then used to pack a mold similar to the one shown in Figure 3.5(b). Similarly, foam models were created and used to pack molds to render another set of aluminum parts. Mold packing is much easier with foam models because it does not need to be removed since the molten metal vaporizes it. On the other hand, a 3D-printed part can be re-used, but requires removal from the packed mold.

The mold-packing process (Figure 3.5(b)) is time consuming and requires spatial thinking to understand. As is shown, the part model is used to create a void in the mold by removing it after packing foundry sand around it. For each casting, the cope was inverted and placed on top the

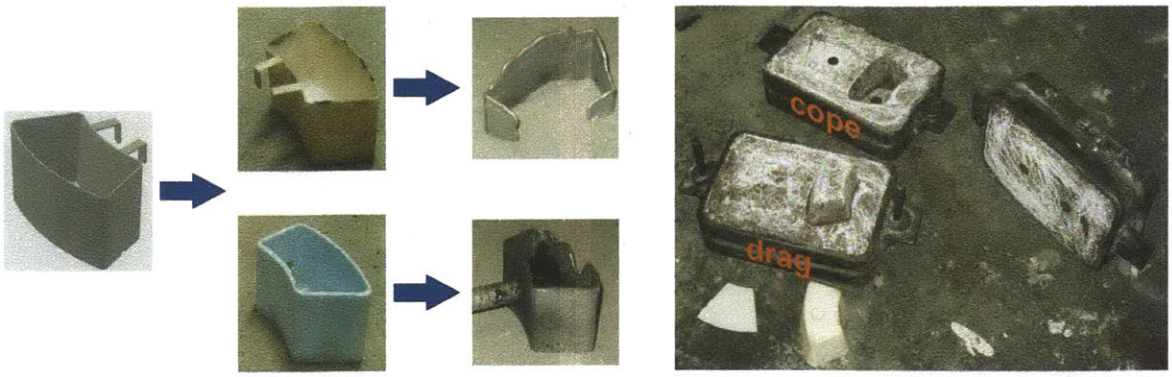

(a) (b)

Figure 3.5: (a) The casting process begins with a digital model and can proceed to a physical part by using a foam or 3D-printed intermediate. (b) Packed sand molds just prior to final assembly and pouring of the molten metal.

drag, while the third flask was stacked on top of these two to provide additional height to drive the molten metal throughout the void.

After many unsuccessful attempts (such as the ones shown in Figure 3.5(a)), a successful cast was finally completed and is shown in Figure 3.6(a). However, the excitement was short-lived because

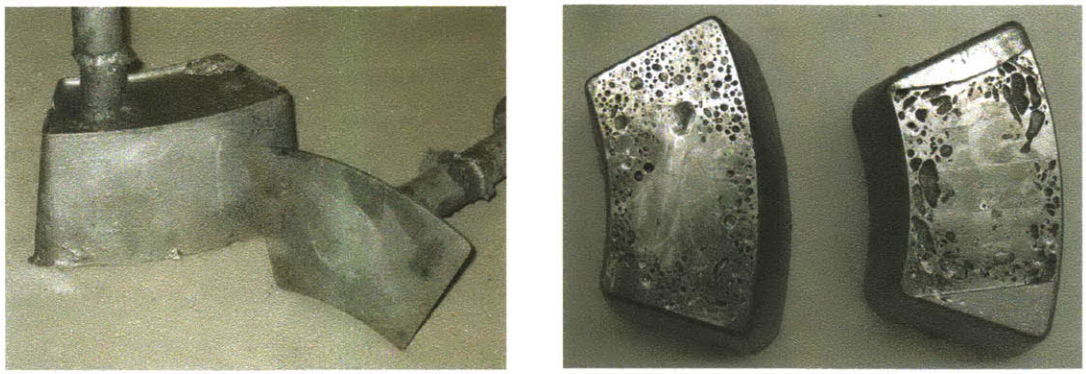

(a) (b)

Figure 3.6: (a) A completed aluminum water vessel and bottom clamping plate using the 3D printed part method. (b) Surface finish after machining the exterior layer of each cast. In the left version, a de-gassing tablet was used to remove hydrogen from the molten metal. On the right, no de-gassing was attempted.

substantial voids were found in the cast (Figure 3.6(b)) as the surface layers were machined flat for module clamping. As is common in aluminum casting, these were caused by dissolved hydrogen to the molten metal from moisture in the air [65]. Since the outer edges of the part freeze first

(because they touch the mold walls), the gas is trapped within the part unless there is venting for it to escape. Degassing tablets were used on the left part of Figure 3.6(b) to remove the gas from the molten metal prior to pouring, but with limited success. The voids were smaller, but were still too numerous for the part to be of use. In the end, the myGen prototype was created using cast aluminum parts from Mystic Valley Foundry in Somerville, Massachusetts.

3.2.2 The Box Extrusion myGen

As an alternative to the casting approach, the box extrusion design of Figure 3.7(a) was implemented and is shown in Figure 3.7(b). Fabrication of this system was very simple and used only

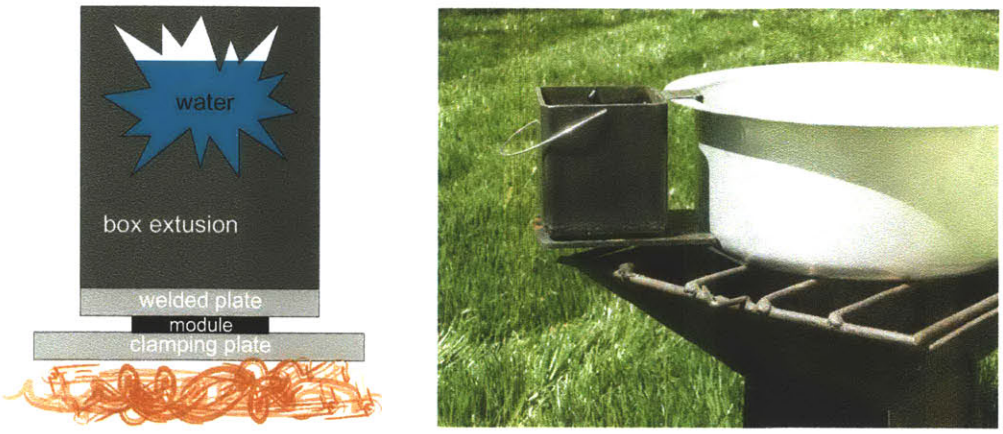

(a) (b)

Figure 3.7: Schematic representation (a) of the box extrusion design which can be fabricated using basic manufacturing techniques. A prototype version is shown in (b).

cutting, welding, drilling, and tapping. Each plate (welded and clamping) was cut to size and drilled with two holes for fastening hardware. The welded plate was joined to the bottom of the box extrusion while the holes in the clamping plate were tapped. The assembly was completed by clamping a Thermonamic 40 x 40 mm module between the two plates with screws, which extended through the welded plate and threaded into the clamping plate. O-rings were used to prevent leakage from the inside of the box extrusion and to allow for module thermal expansion.

The system was then tested for output by heating it over a gas stove. The flowrate was adjusted

for a heat transfer coefficient of 14 $\frac{W}{m^2K}$ and flux of about 1 $\frac{W}{cm^2}$, closely simulating the heating conditions found in Tanzania; 350 mL of water was placed in the box extrusion for cooling. During the test, peak power reached 2 W while connected to a 2.4 Ω load.

To better approximate expected conditions, the box extrusion design was then heated with wood while hooked to the side of a Tanzanian pot resting over a three rock fire. The experimental setup is shown in Figure 3.8. Conditions for this experiment were similar to those of the previous with 350

Figure 3.8: The experimental setup for testing the side-mounted box extrusion design. To simulate field conditions, a three-stone configuration was used with wood as the fuel.

mL of water for cooling with a 2.4 Ω load. As is shown in Figure 3.9(a), however, peak power output reached only 1.4 W corresponding to a temperature differential of about 80°C (Figure 3.9(b)). As indicated by the undulating temperature, current, and voltage curves, the biomass flux was highly variable throughout the test and its low average explains the relatively lower power output. As for the myGen cast design, power output for this system could be improved with a larger heat absorption plate having less contact with the cooking pot.

3.2.3 myGen Manufacturing

The design for high-volume manufacture of myGen systems will likely deviate from those of the prototypes presented here. These were constructed as functional demonstrations, to show that

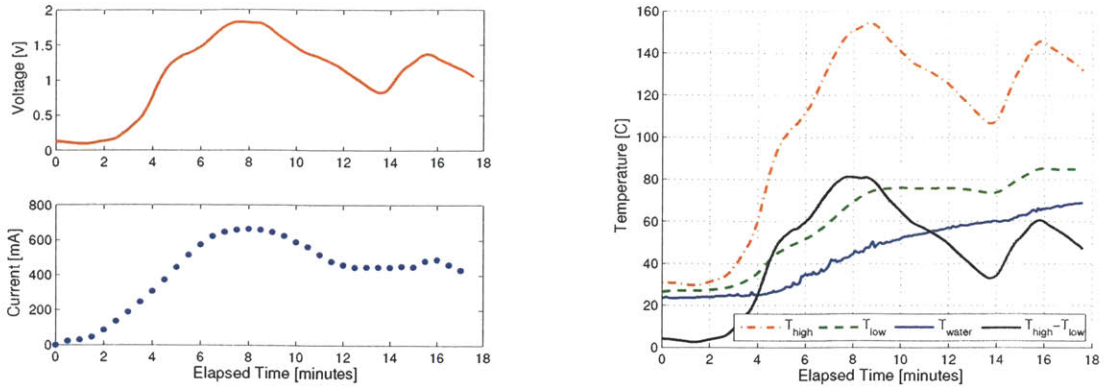

(a) (b)

Figure 3.9: Electrical output (a) and temperature profiles (b) for the box extrusion prototype in a side-mounted position, over a wood fire.

such systems could be created with basic manufacturing techniques like casting, cutting, welding, drilling, and tapping. Although shaping of the plates in both systems was done with the use of a waterjet cutting machine, similar geometries could easily be replicated with a bandsaw or stamping process. Thus, either system could be created in-country if either were preferred to an import approach.

The ultimate decision on importation versus local manufacture is influenced by many variables. First, where is the target market? Does that country have requisite supply chains, manufacturing capabilities, and available labor? Is it in a position for importation from other exporting countries? What is the cost comparison? Have other economic pros and cons been factored in, for example, does in-country manufacture provide substantial job creation for the local labor pool? Such questions need to be answered to determine where and how myGen systems should be manufactured.

In any case, material usage should be minimize to decrease cost and weight without sacrificing lifetime and performance. The system will likely consist of a drawn, thin-walled vessel of aluminum or stainless steel with a robust fin structure for the bottom plate. Each module clamping surface will need to be designed with sufficient stiffness to prevent deflection in order to maintain good thermal interfaces. The design will also need to incorporate a clamping and exit feature for the module's wiring.

Chapter 4

Final Conclusions and Future Work

The intention of this work was to design a personal-scale, off-grid power generation system using thermoelectric technology. To that end, three functional prototypes were developed: Kettlectric and the two myGen systems, the box extrusion and cast aluminum designs. These devices[1] demonstrate success in using thermoelectric technology for off-grid power generation as a by-product of cooking.

These systems offer many advantages to the user. First, they are easy to operate and require no setup or installation. Further, their operation is completely passive, generating electricity as a by-product of cooking. Additionally, they are reliable, high-output power sources that can operate in almost any environmental conditions, provided a cooking fire can be maintained.

Viewing each in more detail, the Kettlectric prototype met more product specifications (Table 1.2) than the myGen systems (Table 3.1). One that fell short for Kettlectric, however, was its power output, averaging 1.4 W which is below the desired 1.5 W. A more significant shortcoming, however, is the anticipated system price due to a high module cost. Even in bulk quantities, it seems unlikely that it could be developed for under $40, let alone $30.

For the myGen systems, many specifications, such as lifetime, burn rate, learning curve, and cooking

[1]Respective technology disclosures were submitted to MIT's Technology and Licensing Office for the Kettlectric and myGen systems.

environment compatibility, were not tested, but are expected to be satisfied. However, the roughly 2 W of peak power output provided by the two myGen designs is unlikely to re-charge the average mobile in under an hour. This could be accomplished with a sustained 3.5 W as suggested by the many mobile power cords sampled. Nor will the price-point be achieved, again due to a high module cost. However, financing schemes are possible, so it is useful to assess payback period.

Assuming a $20 system cost and competitive mobile re-charge rate of 300 Tanzanian Shillings ($0.23), an owner would recover his or her investment in under three months if seven phones were charged per week[2]. If the system cost doubles to $40 and eight phones were charged weekly, payback would take five months.

However, what would be the required module price for a $20 product? For an approximate estimate, the price is first scaled by four to account for retail markup, distribution, and transport; this requires that each system be made for $5. With $1 allotted to overhead and $2 to other system components, each module would need to be purchased for $2. At 3.5 W of output–the estimated requirement for a one hour mobile re-charge–the cost to power ratio becomes $0.57 per watt. As a reference point, Thermonamic sells its module TEP1-1264-1.5 for $8.80 in quantities of 10,000. As tested, it can provide up to 3.5 W under expected operating conditions giving a ratio of $2.51 per watt, or 4.4 times the desired ratio.

Although current power generation modules are priced too high for this application, future demand may drive down cost [66]. This is the opinion of MIT Professor Gang Chen, an expert in the field of thermoelectrics. He acknowledges that low-temperature modules are already available for $0.60 per watt and as low as $2 per module, but duplicating this pricing for high-temperature versions is a matter of increased demand and not materials nor manufacturing process breakthroughs. It is thus encouraging that power generation modules are being considered for waste heat recovery in automobiles [67]. Additionally, the startup Alphabet Energy [68] is claiming power generation for about $1 per watt using, as some speculate, silicon nanowires [69].

Assuming significant cost reductions, improvements to both the product and business model would

[2]This and the next calculation assume there are 4.5 weeks per month.

be required for a successful venture. Future work should focus first on better identifying a target location and customer. Relevant regions will likely have a large number of off-grid mobile users with limited options for recharging. With location selected, a target customer base can then be identified in order to inform willingness to pay and system size (whether for personal use or income generation), among other things.

Selecting a target region will also drive product design since it dictates the manufacturing model. Local manufacture may motivate a cast metal system, or one made of more basic geometries such as in the box extrusion design of myGen. This design could also include the use of car parts or utilize other second-use materials. On the other hand, greater design freedom would be allowed for an imported product, which would likely use a drawn metal vessel with fin structures on the clamping plate to increase heat transfer. In all cases, the clamping surfaces must be designed to maintain thermal contact with the module.

Effort also needs to be directed toward developing the electronic system. This includes the charging circuit, over-temperature alarm, and mobile phone compatibility features. The latter could be accomplished by upping the voltage to a level for use with a "wall" charger or by providing specialty connectors that are compatible with each type of phone.

Apart from product development, distribution, advertising, and repair schemes will need to be optimized. Distribution will be inherently difficult since the target customers are generally dispersed in remote areas. Thus, reaching villages directly will be extremely expensive. One strategy to alleviate cost might be to send products with those already traveling there, such as with bus drivers or truckers. Alternatively, distribution could extend only to major cities which would then require villagers to travel there for purchase. In fact, this is not uncommon, and many travel several hours into town to access goods and services offered there. An effective advertising initiative is also important such that potential customers can be notified of the product's existence as well as to guarantee that they know how to use it. Finally, a repair system is required to maintain the products and customer satisfaction.

In the end, delivering Kettlectric or myGen systems will be more about developing a robust business model than the technology itself.

Bibliography

[1] Eric Martinot and Akanksha Chaurey and Debra Lew and Jos Roberto Moreira and Njeri Wamukonya. Rewnewable Energy Markets in Developing Countries. *Annual Review of Energy and the Environment*, 27:309–348, 2002.

[2] Annual Electric Generator Report - Nonutility 1999. Technical Report EIA-860B, Energy Information Administration, 1999.

[3] World Energy Outlook: Access to Electricity. Technical report, International Energy Agency, 2010.

[4] Katie Fehrenbacher. EGG Energy: The Netflix of Batteries for the Developing World. *http://www.earth2tech.com*, 2010.

[5] Keith Bradsher. Paying in Pollution for Energy Hunger. *The New York Times*, 2007.

[6] Kilian Reiche, Alvaro Covarrubias, and Eric Martinot. *Expanding Electricity Access to Remote Areas: Off-Grid Rural Electrification in Developing Countries*, pages 52–60. World Power, 2000.

[7] Energy Team: Office of Infrastructure and Engineering. An Introductory Guide for Assessing the Potential of Biofuels in Developing Countries. Technical report, US Aid, 2007.

[8] Anilla Cherian. Bridging the Divide Between Poverty Reduction and Climate Change Through Sustainable and Innovative Energy Technologies. Technical report, United Nations Development Programme, 2009.

[9] The Bloom Box: An Energy Breakthrough? CBS 60 Minutes, February 2010.

[10] Bloom Energy. http://www.bloomenergy.com/.

[11] EGG Energy. http://www.egg-energy.com/.

[12] D.Light Design. http://www.dlightdesign.com/.

[13] Humdinger Wind Energy. http://www.humdingerwind.com/.

[14] Rida Y. Nuwayhid, Alan Shihadeh, and Nesreen Ghaddar. Development and testing of a domestic woodstove thermoelectric generator with natural convection cooling. *Energy Conversion and Management*, 46(9-10):1631–1643, 2005.

[15] R.Y. Nuwayhid, D.M. Rowe, and G. Min. Low cost stove-top thermoelectric generator for regions with unreliable electricity supply. *Renewable Energy*, 28(2):205–222, 2003.

[16] D. Champier, J.P. Bedecarrats, M. Rivaletto, and F. Strub. Thermoelectric power generation from biomass cook stoves. *Energy*, 35(2):935 – 942, 2010. ECOS 2008, 21st International Conference, on Efficiency, Cost, Optimization, Simulation and Environmental Impact of Energy Systems.

[17] David Hegarty. Satisfying a burning need. *Password: Philips Research Technology Magazine*, 28:28–31, 2006.

[18] R.Y. Nuwayhid and R. Hamade. Design and testing of a locally made loop-type thermosyphonic heat sink for stove-top thermoelectric generators. *Renewable Energy*, 30(7):1101–1116, 2005.

[19] Taihuaxing Thermoelectric Module. http://www.thermonamic.com/home.html.

[20] Termo-Gen AB. http://www.termo-gen.com.

[21] Vice Presidency for Sustainable Development. An Investment Framework for Clean Energy and Development: A Progress Report. Technical report, The World Bank, sept 2006.

[22] Generator Sales. Diesel Generators for Home Power or Off-Grid Electricity. http://www.generatorsales.com/diesel-generators.asp.

[23] Brooke Crothers. Bloom Energy tech 'not unique,' analyst says. *CNET News*, 2010.

[24] Peter Luis. Personal communication, January 2010.

[25] Saning'o Kimani. Personal communication, January 2010.

[26] Lon Bell. Cooling, Heating, Generating Power, and Recovering Waste Heat with Thermoelectric Systems. *Science*, 321(5895):1457–1461, September 2008.

[27] Bart Van Zeghbroeck. *Principles of Semiconductor Devices.* University of Colorado, 2007.

[28] eHow. http://www.ehow.com.

[29] Francis J. DiSalvo. Thermoelectric Cooling and Power Generation. *Science*, 285(5428):703–706, 1999.

[30] Thermoelectric Power Generator Design and Selection from TE Cooling Module Specifications. Technical report, TE Technology, Inc.

[31] Chuang Yu and K.T. Chau. Thermoelectric automotive waste heat energy recovery using maximum power point tracking. *Energy Conversion and Management*, 50:1506-1512, Apr 2009.

[32] All Electronics. http://www.allelectronics.com/.

[33] DigiKey Corp. - Electronic Components Distributor. http://www.digikey.com/.

[34] Thomas Szepesi and Kin Shum. Cell phone power management requires small regulators with fast response. *Planet Analog*, 2002.

[35] CustomThermoelectric - Your Thermoelectric Partner. http://www.customthermoelectric.com/.

[36] Tellurex: Thermal Leader in Thermoelectric Solutions. http://tellurex.com/.

[37] Marlow Industries, Inc. http://www.marlow.com.

[38] Vaclav Smil. *Energy in Nature and Society: General Energetics of Complex Systems.* The MIT Press, 2008.

[39] Amy Smith. Personal communication, November 2009.

[40] Dennis Nagle. Personal communication, October 2009.

[41] The World Bank. http://web.worldbank.org, 2009.

[42] Andreas Kemmler. Factors influencing household access to electricity in india. *Energy for Sustainable Development*, 11(4):13 – 20, 2007.

[43] Green Power For Mobile: Charging Choices: Off-grid charging solutions for mobile phones. Technical report, GSMA Development Fund, October 2009.

[44] Paul Polak. *Out of Poverty.* Berrett-Koehler Publishing, Inc., 2008.

[45] Jeff Zira. Target Country Matrix. Personal Communication.

[46] NASA Earth Observations. http://neo.sci.gsfc.nasa.gov/Search.html.

[47] United Nations Data. Population using solid fuels, percentage.

[48] E. Cravalho, J. Smith, J. Brisson, and G. McKinley. *Thermal-Fluids Engineering.* Oxford University Press, Cambridge, Massachusetts, Fall 2006 edition, 2005.

[49] Kalyan Annamalai and Ishwar Kanwar Puri. *Combustion Science and Engineering.* CRC Press, 2006.

[50] Air BP: Handbook of Products, 2000.

[51] Michael F. Ashby. *Materials Selection in Mechanical Design.* Elsevier, third edition, 2005.

[52] Nidal H. Abu-Hamdeha and Randall C. Reederb. Soil Thermal Conductivity. *Soil Science Society of America Journal*, 64:1285–1290, 2000.

[53] K N R Taylor. Thermal expansion of bismuth telluride. *British Journal of Applied Physics*, 12(12):717, 1961.

[54] Cotronics Corp. - Provider of High Temperature Materials. http://www.cotronics.com/.

[55] A.F. Mills. *Heat and Mass Transfer.* Irwin, 1995.

[56] Isidor Buchmann. *Batteries in a Portable World.* Cadex Electronics, Inc., second edition, 2001.

[57] Sanyo. http://battery.sanyo.com/.

[58] RadioShack. http://www.radioshack.com/.

[59] Maxim Integrated Products. http://www.maxim-ic.com/.

[60] Make Magazine. http://www.makezine.com/.

[61] Colin Mitchell's Talking Electronics. http://www.talkingelectronics.com.

[62] http://www.1.bp.blogspot.com. http://www.1.bp.blogspot.com.

[63] Cell phone power management requires small regulators with fast response. http://www.planetanalog.com/showArticle.jhtml?articleID=12801994.

[64] Jodie Wu. Personal communication, November 2009.

[65] American Foundry Society, Inc. Controlling Aluminum Gas Porosity. http://thefreelibrary.com.

[66] Professor Gang Chen. Personal Communication, April 2010.

[67] U.S. Department of Energy: Energy Efficiency and Renewable Energy. http://www.eere.energy.gov/.

[68] Alphabet Energy. http://www.alphabetenergy.com/.

[69] Michael Kanellos. 'Silicon + Heat = Cheap Energy' Gets $1 Million.